2,2′-Bithiophene Radical Cation: An Experimental and Computational Study

Tamás Keszthelyi,*,† Mette M.-L. Grage, Jesper F. Offersgaard,‡ and Robert Wilbrandt§

Condensed Matter Physics and Chemistry Department, FYS-313, Risø National Laboratory, DK-4000 Roskilde, Denmark

Christian Svendsen|| and O. Sonnich Mortensen⊥

Physics Department, Odense University, DK-5230 Odense M, Denmark

Jesper K. Pedersen and Hans Jørgen Aa. Jensen

Chemistry Department, Odense University, DK-5230 Odense M, Denmark

Received: November 5, 1999; In Final Form: December 3, 1999

Electronic absorption and resonance Raman spectra of the radical cation of bithiophene are reported. The bithiophene radical cation was produced by γ-radiolysis in a glassy matrix at 77 K, and the Raman spectrum excited in resonance with the two absorption bands at 425 and 590 nm. The electronic states relevant to the observed electronic transitions were identified and characterized by CASSCF calculations. The optical absorption and resonance Raman spectra were calculated by wave packet propagation methods using the ab initio calculated molecular parameters. The calculated spectra agree well with the experimental ones. The importance of carrying out full wave packet propagation calculations is underlined by the fact that in one case the simple Savin formula gave a completely wrong prediction of the resonance Raman spectrum.

Introduction

In recent years, conjugated polymers have received much attention for their properties such as electrical conductivity, photoconductivity, electroluminescence, and fast nonlinear optical response.[1] Polythiophenes and substituted polythiophenes have been studied extensively in this context.[2] Since they have a nondegenerate ground state they carry the possibility of self-localized excitations such as polarons (radical ions) and bipolarons (doubly charged ions)[3] that may in turn act as charge carriers. It is therefore interesting to examine the radical cations and dications of the oligothiophenes as models of polythiophene. The radical cations of the oligomers from bithiophene to sexithiophene have been photochemically generated and their absorption spectra measured,[4,5] the radical cation of sexithiophene has furthermore been generated by photoexcitation[6] and the Raman spectra of sexithiophene, its radical cation, and its dication have been compared to Raman spectra of doped and undoped polythiophene.[7] Attempts to make stable substituted oligothiophene radical cations have also been reported.[8] Dications have been investigated theoretically for oligothiophenes with two to five rings[9] and experimentally for six rings.[5] Substituted oligothiophene radical cations and dications have been generated.[10]

2,2′-Bithiophene ($(C_4H_3S)_2$ in the following referred to as bithiophene, 2T) can be seen as the smallest model compound of polythiophene and it is interesting to know the geometry and vibrational structure of its radical cation, $2T^{+\bullet}$. We have recently reported preliminary results of the resonance Raman spectrum of the photochemically generated radical cation in solution together with an assignment based on density functional theory calculations of the vibrational frequencies.[11] In the present communication, we report the extension of these studies to the electronic absorption spectrum of the bithiophene radical cation, generated by γ-radiolysis in a low-temperature Freon glass, together with its resonance Raman spectrum excited at 425 and 550 nm, in resonance with two different electronic transitions. Results of molecular orbital calculations of ground and excited state properties, and time-dependent wave packet propagation calculations of the absorption and resonance Raman spectra are also presented.

Experimental and Theoretical Methods

Materials. 2,2′-Bithiophene of purity 97% and fumaronitrile of purity 98% were purchased from Aldrich and used without further purification. The solvents employed were obtained from different sources, namely acetonitrile (Supergradient, HPLC) from Lab-Scan, $CFCl_3$ (Freon-11) from Aldrich, and $BrCF_2$-CF_2Br (Freon-114B2) from Fluorochem. Acetonitrile was used without purification, while the Freons were dried on 5 Å molecular sieves.

Generation of the Radical Cations. For the low-temperature measurements 10^{-2} M solutions of 2T in an air-saturated 1:1 (v/v) mixture of the above Freons were prepared. Upon cooling to 77 K, the samples formed transparent glasses. For measuring electronic absorption spectra the glasses were irradiated with a dose of 0.01 Mrad by ^{60}Co γ-rays, while doses of 0.1−0.3 Mrad

* Corresponding author.
† Present address: Chemistry Department, Aarhus University, Langelandsgade 140, DK-8000 Århus C, Denmark.
‡ Present address: DELTA Light & Optics, Hjortekærsvej 99, DK-2800 Lyngby, Denmark.
§ Present address: Bornholms Amtsgymnasium, Søborgstræde 2, DK-3700 Rønne, Denmark.
|| Present address: Danfoss Compressors, Mads Clausen Strasse 7, D-24939 Flensburg, Germany.
⊥ Present address: Institute of Applied Physics, SDU−Odense University/The Engineering College of Odense, Niels Bohrs Allé 1, DK-5230 Odense M, Denmark.

10.1021/jp993913s CCC: $19.00
Published on Web 03/01/2000

were used for the resonance Raman measurements. The samples were then transferred to an Oxford Instruments DN1704 liquid nitrogen cryostat to perform the optical measurements. The samples were prepared in 10 mm inner diameter cylindrical and 10×10 mm^2 rectangular quartz cells to record resonance Raman and electronic absorption spectra, respectively. During the resonance Raman measurements the cells were rotated at 8 rpm in the cryostat.

For the time-resolved resonance Raman experiments air-saturated room-temperature solutions of 10^{-3} M bithiophene and 0.1 M fumaronitrile were prepared in cylindrical Suprasil cells with 26 mm inner diameter and 6 mm inner height. The sample cell was rotated during measurements. The radical cations were in this case produced via a photoinduced electron transfer reaction between excited bithiophene and the electron acceptor fumaronitrile. A 248 nm pulse of 20 ns duration from an excimer laser (Lambda Physik LPX200i) was used as pump. The pump energy was approximately 10 mJ per pulse on the sample.

Detection of the Radical Cations. Resonance Raman spectra were recorded at excitation wavelengths of 425 and 550 nm. 425 and 550 nm laser radiation of 1.0−2.0 mJ per pulse (15 ns pulses, 25 Hz repetition rate) was obtained from an excimer (Lambda Physik EMG 102E) pumped dye laser (Lambda Physik FL3002, Stilbene-420 or Coumarin-540A laser dye).

The probe beam was focused on the sample cell by a cylindrical lens. Pump−probe delay in the time-resolved experiments was typically 90 ns.

In the 550 nm experiments, the scattered Raman light was collected at right angles by achromatic lenses and focused onto the vertical entrance slit of a home-built 0.6 m Czerny−Turner single monochromator (1200 grooves/mm ruled grating) through a SN550 holographic notch filter (Kaiser Optical Systems) and a polarization scrambler.

In the 425 nm low-temperature experiments, the scattered light was collected in a backscattering geometry and analyzed in a commercial spectrometer (Jobin-Yvon T64000), used together with its double subtractive premonochromator (1200 grooves/mm gratings, blazed at 630 nm). A polarization scrambler was placed in front of the spectrometer, but no band-pass filter was used.

The 425 nm time-resolved experiments were carried out in a 90° scattering geometry using the Jobin-Yvon spectrometer in single mode.

A slit width of 0.2 mm was used in all the experiments, resulting in a spectral resolution of 11 cm^{-1} at 425 nm and 8 cm^{-1} at 550 nm. The spectra were in all the experiments detected by a gated optical multichannel analyzer, with 700 active channels (Spectroscopy Instruments OSMA IRY-700). They were calibrated either in wavenumber, using the Raman spectrum of indene as a reference, or in wavelength using rare-gas emission lines.

Data collection was controlled by a PDP11/23 computer and subsequent data handling performed on a PC. The spectral range of interest was covered combining several spectra. In the low-temperature measurements, a sample was usually exposed to 5000−15000 laser pulses. Spectra of the samples in the Freon mixture at 77 K without γ-irradiation were also recorded and digitally subtracted from the spectra obtained from γ-irradiated samples, using empirical scaling factors. In the time-resolved resonance Raman experiments one cell of sample was typically exposed to 2400 pulses and the final spectrum was collected on two to three cells. For each cell a probe-only spectrum was also recorded and later subtracted from the pump-and-probe spectrum.

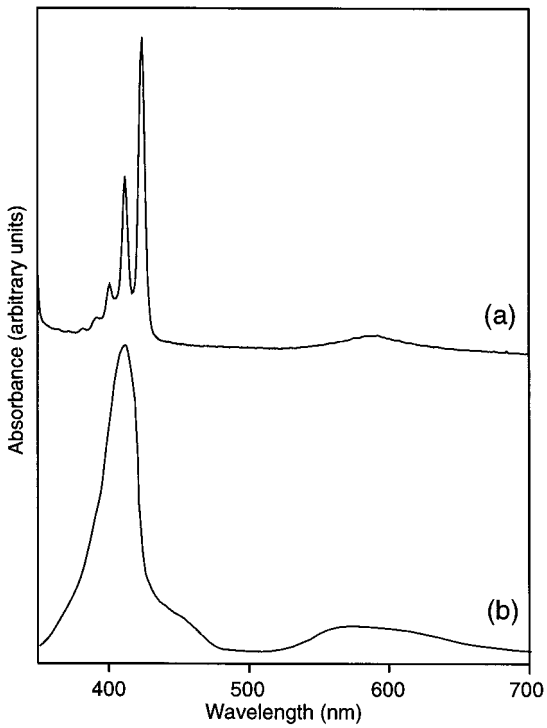

Figure 1. Electronic absorption spectrum of the radical cation of bithiophene, generated (a) radiolytically in a low-temperature glassy matrix (this work) and (b) photochemically in acetonitrile solution (adapted from ref 4).

In the present experimental work, we have not attempted to obtain quantitative Raman intensities. The spectra are not corrected for the reabsorption of the scattered light by the radical cation, neither for the wavelength dependence of the sensitivity of the collection optics and the detection system. However, because all these effects can be expected to be smooth functions of wavelength, and in part cancel each other, the observed relative intensity pattern should be qualitatively acceptable.

Computational Tools. Molecular orbital calculations were performed by density functional theory (DFT) and by the complete active space self-consistent field (CASSCF) method.

The DFT calculations were carried out using the UB-LYP and UB3-LYP methods and the standard 6-31G* basis set. At this level of theory geometry optimizations were carried out for neutral bithiophene and its radical cation, and vibrational frequencies were calculated at each of the optimized geometries using analytical derivative techniques. These calculations were performed using the Gaussian 94 suite of programs.[12] The 6-31G* basis set and the exchange and correlation functionals were used as contained in the program.

CASSCF calculations were carried out for planar forms of the radical cation of bithiophene. The active space was selected on the basis of MP2 natural orbital occupation numbers[13] and comprised the 10 valence-π orbitals containing 11 active electrons. Geometry optimizations and subsequent vibrational analyses were performed for the ground and some excited states of s-trans (C_{2h}) and s-cis (C_{2v}) $2T^{+\bullet}$ relevant to the experimental results. These excited states have been selected based on the results of multiconfigurational linear response calculations of transition energies and oscillator strengths at the ground state optimized geometries. All CASSCF calculations were performed by the DALTON program[14] using the 6-31G* basis set.

Results and Discussion

Experimental Results. The upper trace of Figure 1 shows

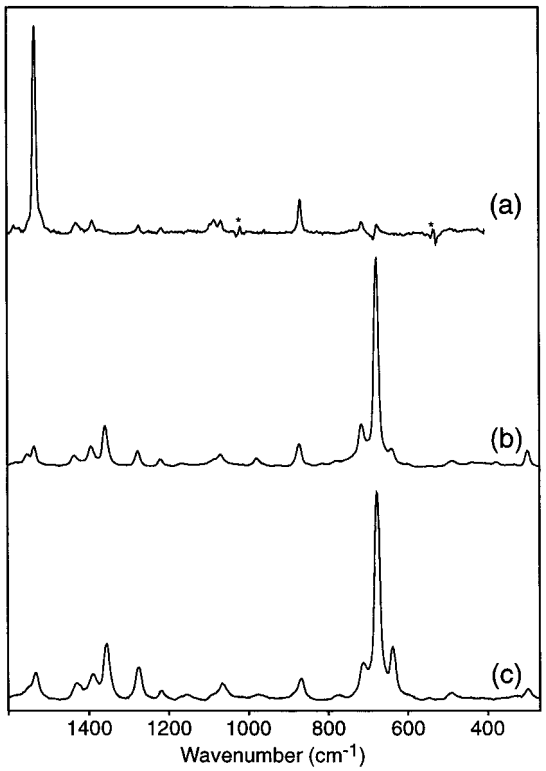

Figure 2. Comparison of the resonance Raman spectra of the bithiophene radical cation recorded in different media and at different excitation wavelengths: (a) in Freon glass at 550 nm; (b) in Freon glass at 425 nm; (c) in acetonitrile solution at 425 nm.

the electronic absorption spectrum of the bithiophene radical cation created by γ-irradiation of bithiophene in a Freon matrix at 77 K. The spectrum consists of a relatively weak structureless band at 590 nm and a strong one at 425 nm, the latter exhibiting a vibrational progression of $\sim$680 cm^{-1}. This absorption spectrum is very similar, although with considerably more pronounced vibronic structure in the higher energy band, to that of the photochemically generated radical cation,[4] reproduced in the lower trace of Figure 1.

We recorded Raman spectra in resonance with both absorption bands. Figure 2 shows the resonance Raman spectrum in the 275−1600 cm^{-1} wavenumber range of radiolytically generated $2T^{+\bullet}$ excited at 550 and 425 nm, together with the 425 nm excited Raman spectrum of the photochemically generated radical cation.[11] The Raman spectra measured in resonance with the two electronic transitions are very different (parts a and b of Figure 2), whereas the spectra obtained at the same excitation wavelength in the glass and in solution are very similar (parts b and c of Figure 2). Even though the 550 nm excitation wavelength is at considerably higher energy than the 590 nm absorption maximum, we argue to consider the spectrum excited at 550 nm be resonant with the low-energy electronic transition of the bithiophene radical cation. One reason for this is that we have measured Raman spectra (not shown here) using 600 nm excitation, very close to the absorption maximum, and these spectra are very similar to the one measured at 550 nm excitation. The good agreement between experimental and simulated spectra (see below) further substantiates this argument. Figure 3 shows the 425 nm excited resonance Raman spectrum of the radiolytically generated bithiophene radical cation in the 275−2300 cm^{-1} wavenumber region. In this spectral range, a number of overtone and combination bands are observed.

Neutral Bithiophene. Neutral 2T was shown by gas-phase electron diffraction[15] to exist in two nonplanar conformations, s-trans-gauche and s-cis-gauche, with relative abundances of 56 $\pm$ 4% and 44 $\pm$ 4% and torsional angles of 148 $\pm$ 3° and 36 $\pm$ 5°, respectively. The geometrical structure and torsional potential of neutral 2T have recently been studied by the group of Ortí, using ab initio HF and MP2[16] and DFT[17] calculations. (Reference 16 also gives a review of the experimental and theoretical studies of the conformational isomerism of 2T). These calculations agree with the electron diffraction results in predicting nonplanar s-trans-gauche and s-cis-gauche conformations. The geometrical parameters obtained by electron diffraction[15] are listed in the first column of Table 1. (See Figure 4 for the numbering of atoms.) It should be noted here that Ortí et al. have suggested a revision, at least in terms of the bond lengths, of the electron diffraction data of ref 15.

We have carried out geometry optimizations for the two conformers of neutral 2T at the UB-LYP and UB3-LYP levels using the 6-31G* basis in order to be able to compare the calculated geometrical parameters with those obtained for the radical cation. Our calculations also yield nonplanar conformers (C_2 symmetry). Planarity of the individual thiophene rings was not forced in these calculations, nevertheless the deviation from planarity is less than 1° for all intraring dihedral angles. The geometrical parameters are listed in the third and fourth columns of Table 1. (See Figure 4 for the numbering of atoms.) There is good qualitative agreement between our UB-LYP and UB3-LYP results and the experimental[15] and MP2[16] geometries. The torsional angles for the s-trans-gauche and s-cis-gauche conformers calculated by UB-LYP (162.4° and 29.1°) and UB3-LYP (157.4° and 32.2°) are closer to planarity than the experimental (148° and 36°)[15] and MP2 (142.2° and 43.3°)[16] ones but agree well with the B3-P86 (159.0° and 29.3°) and B3-PW91 (157.4° and 30.8°)[17] values. This preference of planar to perpendicular conformers by DFT methods has been discussed in ref 17. The energy difference between the s-trans-gauche and s-cis-gauche conformers is predicted as 2.80 kJ/mol by UB-LYP and 2.86 kJ/mol by UB3-LYP. This should be contrasted by the values of 2.13, 2.99, and 2.90 kJ/mol obtained at the MP2,[16] B3-P86, and B3-PW91[17] levels, and the experimental estimates of 0.75 kJ/mol from electron diffraction[15] and 4.85 $\pm$ 0.54 kJ/mol from fluorescence[18] data. As far as the calculated bond lengths are concerned, the MP2 values for the carbon−sulfur bond lengths are much closer to the experimental ones than the UB-LYP and UB3-LYP ones. In the $C_2-C_3-C_4-C_5$ fragment, the UB-LYP and especially the UB3-LYP calculations predict a greater degree of bond alternation than the MP2 calculations. The inter-ring $C_2-C_{2'}$ bond length is very close to both the MP2 and the experimental value. On the whole, we find that the UB-LYP and UB3-LYP calculations are able to give a good qualitative description of the geometrical structures of the two stable conformers of neutral bithiophene. In the next section, these structures will be compared to the ones obtained at the same level of theory for the radical cation of bithiophene.

Geometry of the Radical Cation in the Ground State. To our best knowledge, there is no experimental structure available in the literature for the bithiophene radical cation. We have carried out geometry optimizations at the UB-LYP, UB3-LYP, and CASSCF levels using the 6-31G* basis set. The optimizations were carried out in the C_{2v} point group for the planar s-cis and in the C_{2h} point group for the planar s-trans form of the radical cation. Subsequent calculations of the vibrational frequencies yielded all real values, indicating that the planar structures are real minima on the potential energy surface of $2T^{+\bullet}$. The energy difference between the s-trans and the higher

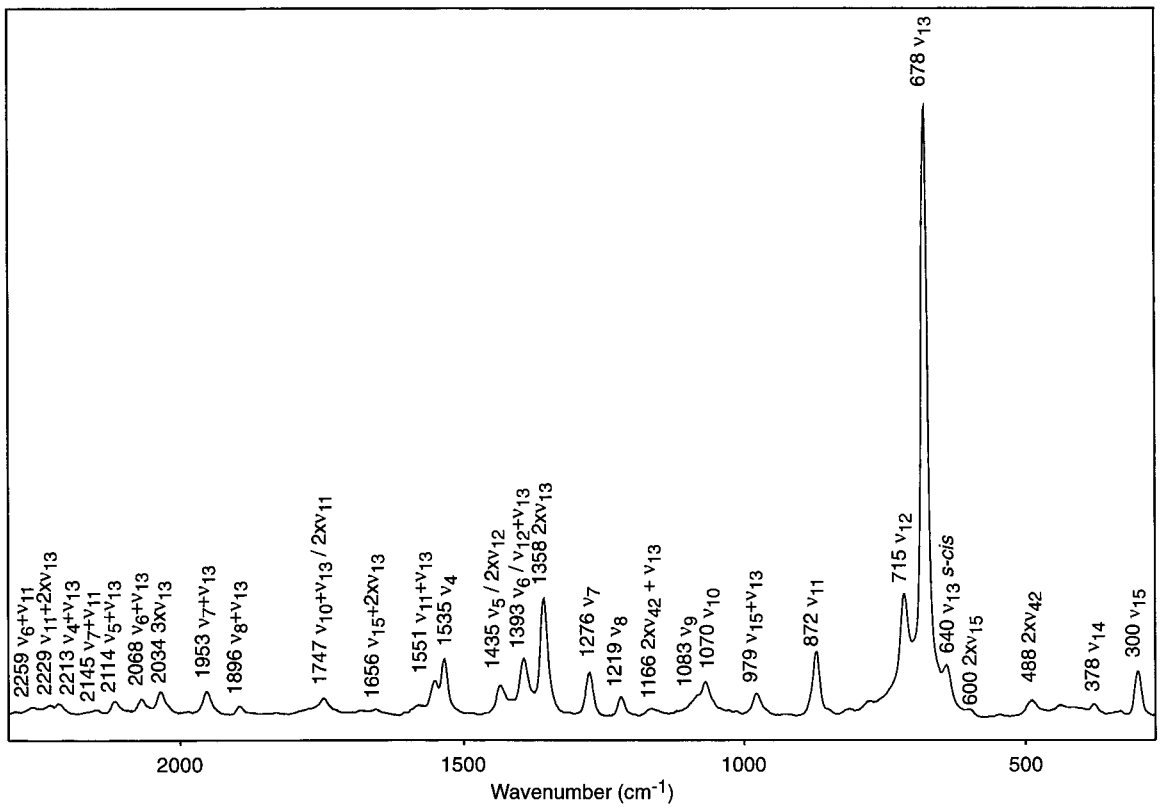

Figure 3. The 425 nm excited resonance Raman spectrum of the radiolytically generated bithiophene radical cation in the 275−2300 cm^{-1} wavenumber range. The positions and assignments of the Raman bands are indicated.

TABLE 1: Calculated Geometrical Parameters for s-trans and s-cis Neutral Bithiophene and Ground State Bithiophene Radical Cation (Bond Lengths in Ångströms, Bond Angles and Dihedral Angles in Degrees)

	neutral			radical cation		
	exptl[a]	UB-LYP	UB3-LYP	UB-LYP	UB3-LYP	CASSCF
			s-trans			
$r_{22'}$	1.456	1.453	1.451	1.416	1.406	1.399
r_{12}	1.733	1.780	1.756	1.794	1.770	1.737
r_{15}	1.719	1.754	1.736	1.732	1.715	1.708
r_{45}	1.363	1.379	1.368	1.406	1.396	1.392
r_{34}	1.452	1.430	1.424	1.401	1.391	1.389
r_{23}	1.370	1.391	1.378	1.424	1.416	1.421
$\alpha_{122'}$	121.9	120.7	120.8	121.3	121.7	122.7
α_{215}	91.7	91.6	91.8	90.7	90.9	91.6
α_{154}	112.3	111.6	111.6	113.2	113.3	112.9
α_{345}	112.3	113.1	112.9	112.6	112.4	112.2
α_{234}	111.9	113.9	113.6	113.4	113.2	113.0
α_{123}	111.8	109.8	110.1	110.1	110.2	110.3
$d_{122'1'}$	148 ± 3	162.4	157.4	180.0	180.0	180.0
			s-cis			
$r_{22'}$	1.456	1.456	1.453	1.417	1.407	1.400
r_{12}	1.733	1.778	1.755	1.790	1.766	1.735
r_{15}	1.719	1.753	1.735	1.733	1.717	1.710
r_{45}	1.363	1.380	1.368	1.406	1.395	1.391
r_{34}	1.452	1.430	1.424	1.401	1.391	1.390
r_{23}	1.370	1.391	1.378	1.427	1.418	1.423
$\alpha_{122'}$	121.9	122.1	122.2	122.8	123.0	123.8
α_{215}	91.7	91.7	91.8	90.8	90.9	91.7
α_{154}	112.3	111.5	111.6	113.1	113.2	112.9
α_{345}	112.3	113.1	112.9	112.7	112.5	112.2
α_{234}	111.9	113.8	113.5	113.3	113.2	112.9
α_{123}	111.8	109.9	110.2	110.1	110.2	110.3
$d_{122'1'}$	36 ± 5	29.1	32.2	0.0	0.0	0.0

[a] Electron diffraction data from ref 15. A revision, at least in terms of the bond lengths, of these data has been suggested by Ortí et al.[16]

energy s-cis forms is predicted as 2.82 kJ/mol by UB-LYP, 2.72 kJ/mol by UB3-LYP, and 1.95 kJ/mol by CASSCF, the same order of magnitude as for neutral bithiophene. The geometrical parameters obtained are listed in the fifth through seventh columns of Table 1. (See Figure 4 for the numbering of atoms.)

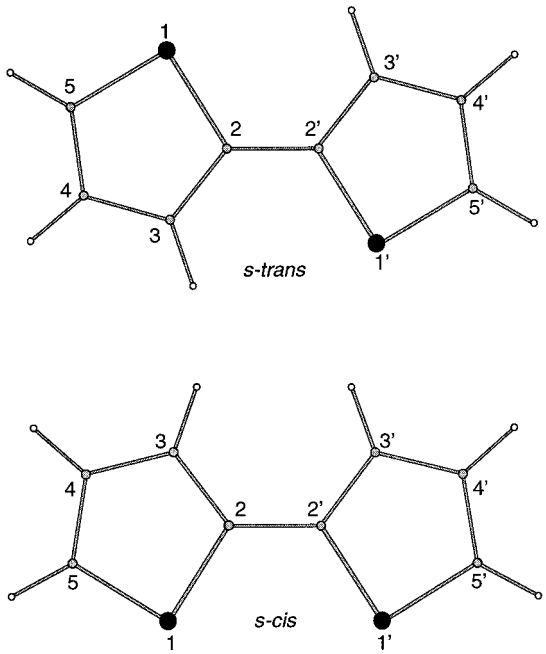

Figure 4. Numbering scheme for the definition of geometrical parameters for the two conformers of neutral bithiophene and the two rotamers of its radical cation.

The two DFT methods yield similar structures, the calculated C−C bond lengths differ by ∼0.01 Å, the S−C bond lengths by ∼0.02 Å, in both cases the UB3-LYP calculations giving the shorter bonds, as expected on the basis of the presence of the HF exchange functional in this hybrid DFT method. The differences in bond angles are 0.1−0.4°. The optimized CASSCF bond lengths for both the s-cis and s-trans forms of the radical cation differ from the UB3-LYP values by at most 0.007 Å, except for the S_1-C_2 bond where the CASSCF value

is 0.033 Å shorter for s-trans and 0.031 Å shorter for s-cis A comparison with the experimental and the two DFT values for neutral bithiophene indicates that the CASSCF value is probably the most accurate, and that the UB-LYP and UB3-LYP calculations give a poorer description of the S atoms than of C and H. The difference between the CASSCF and UB3-LYP bond angles is largest (0.7−1.0°) for the angles involving S_1 and C_2, which is obviously related to the difference in the S_1-C_2 bond length mentioned above. The other bond angles differ by at most 0.4°.

Comparing the UB-LYP and UB3-LYP geometries of neutral bithiophene and its radical cation, the most drastic change is observed in the C−C bond lengths. The $C_2-C_{2'}$ and C_3-C_4 single bonds of the neutral shorten by ∼0.04 Å, while the C_2-C_3 and C_4-C_5 double bonds lengthen by ∼0.03 Å upon ionization, resulting in reversed but considerably less bond alternation in the radical cation than in the neutral. Similar trends were observed in our previous studies of short polyene radical cations.[19] These changes of interatomic distances are in fact to be expected considering the nodal properties of the highest occupied molecular orbital (HOMO) of neutral bithiophene, shown in Figure 5a. Removal of an electron from this orbital, which is bonding along the C_2-C_3 and C_4-C_5 bonds and antibonding along the $C_2-C_{2'}$ and C_3-C_4 bonds, is expected to result in the elongation of the former and shortening of the latter bonds, as born out by our DFT calculations. The S−C bond lengths change by smaller amounts, an ∼0.01 Å increase of the S_1-C_2, and an ∼0.02 Å decrease of the S_1-C_5 bond lengths takes place when going from the neutral to the radical cation, in agreement with the small amplitude at the two S atoms for the HOMO.

Because of the increase of the double-bond character of the inter-ring $C_2-C_{2'}$ bond, expressed by the shortening of this bond, we prefer to use the neutral term "rotamers" in reference to the stable forms of $2T^{+\bullet}$.[20] As a consequence of this increase in double bond character, there appears to be no gauche minima for the radical cation, and the barrier for the interconversion of the s-trans and s-cis forms is expected to be higher than the one separating the s-trans-gauche and s-cis-gauche conformers of neutral bithiophene. An even stronger argument for this is delivered by the state correlation diagram of Figure 5d (see below), which strongly predicts planar minima and a high rotation barrier. For the neutral, barrier heights of 6.31, 11.24, and 10.51 kJ/mol were obtained at the MP2,[16] B3-P86, and B3-PW91[17] levels, respectively. An uncorrelated ROHF/6-31G* calculation of the transition state connecting the s-trans and s-cis forms of $2T^{+\bullet}$ gave a barrier height of 752 kJ/mol (relative to the s-trans rotamer) for interconversion of the two forms. Given the limitations of the ROHF model, this value is expected to be too high, but in any case it supports the reasoning that interconversion of the two rotamers of the radical cation is highly unlikely in the low-temperature samples.

Electronic Structure and Transitions of the Radical Cation. *Qualitative Description.* We can obtain a qualitative description of the low-lying electronic states of the 2T radical cation from the schematical π-molecular orbital diagram of neutral 2T, shown in Figure 5a. The lowest energy excited states are expected from excitations within the π orbital manifold. In the C_{2h} point group of the s-trans rotamer, these orbitals are in order of increasing energy $2a_u$, $2b_g$, $3a_u$, $3b_g$, $4a_u$, and $4b_g$, with orbital energies (or Koopmans' vertical ionization energies if taken with opposite sign) of −14.9, −13.7, −10.1, −9.7, −9.4, and −7.0 eV (ROHF/6-31G* values at the optimized geometry of s-trans $2T^{+\bullet}$). Thus, the ground state of the 2T radical cation is expected to be a ^2B_g state arising from the removal of one electron from the highest occupied molecular orbital of neutral 2T. One electron excitations from the doubly occupied $4a_u$, $3a_u$, and $2a_u$ orbitals to the singly occupied $4b_g$ orbital of the radical cation give rise to ^2A_u states, and so do excitations from this orbital to the $5a_u$ and $6a_u$ unoccupied orbitals. Of these excitations, the $4a_u \rightarrow 4b_g$, $3a_u \rightarrow 4b_g$, and $4b_g \rightarrow 5a_u$ excitations are expected to contribute significantly to the lowest-lying ^2A_u excited states. The $^2B_g \rightarrow {}^2A_u$ transitions are dipole allowed. Similarly, excitations from the $3b_g$ and $2b_g$ orbitals to the singly occupied $4b_g$ orbital, and from the latter to the $5b_g$ and $6b_g$ orbitals give rise to ^2B_g states. However, under C_{2h} symmetry, the $^2B_g \rightarrow {}^2B_g$ excitations are dipole forbidden. Excitations from π to σ orbitals give rise to additional states of A_g and B_u symmetry. The $^2B_g \rightarrow {}^2A_g$ transitions are dipole forbidden, and on the basis of orbital energies the ^2B_u states are expected at significantly higher energies than the low-lying ^2A_u π-states.

Under the C_{2v} symmetry of the s-cis rotamer, the π orbitals are of a_2 and b_1 symmetry. On the basis of the orbital energies of neutral 2T (ROHF/6-31G*, calculated at the C_{2v} optimized geometry of s-cis 2T radical cation), the ground state of the radical cation is expected to be a $^2A_2$ state. One electron excitations within the π-orbital manifold give rise to $^2A_2$ and $^2B_1$ states, transitions to which from the $^2A_2$ ground state are dipole allowed. Excitations from π to σ orbitals give rise to states of A_1 and B_2 symmetry. The $^2A_2 \rightarrow {}^2A_1$ transitions are dipole forbidden and the $^2A_2 \rightarrow {}^2B_2$ are expected at high energies.

Linear Response Calculations. To identify the electronic states observed in the absorption spectrum (Figure 1), we have carried out multiconfigurational linear response calculations of transition energies and oscillator strengths[21] for transitions from the ground state at the CASSCF optimized geometries of both the s-trans and the s-cis rotamer. Transitions from the ground state to the three lowest excited doublet states of each symmetry were considered, and the oscillator strengths were calculated both in the dipole length and the dipole velocity representations. The results are given in Table 2. The symmetry of the excited state is given in the first column, and the calculated energies of the excited states, relative to the ground state, are given in electronvolts, wavenumbers, and nanometers in the third to fifth columns. The last two columns give the oscillator strengths in the dipole length and dipole velocity representations. The oscillator strength values calculated in the two representations are sufficiently close to each other, indicating that all the excitations are adequately described by the basis set used. As expected from our considerations of the molecular orbitals, the excited states of π-character (A_u and B_g for s-trans A_2 and B_1 for s-cis) lie considerably lower in energy than those of σ-character. Also, transitions to the states of σ-character have very low oscillator strengths. On the basis of the calculated transition energies and oscillator strengths, the relevant excited states are of A_u symmetry for the s-trans rotamer and of B_1 symmetry for the s-cis rotamer. In the case of the s-trans rotamer, the first ^2A_u excited-state lies at 1.75 eV (709 nm) above the ^2B_g ground state, and transition to this state from the ground state has an oscillator strength of 0.0032 and 0.0024 in the dipole length and dipole velocity representations, respectively. Transition to this state is much further to the red than the two electronic transitions we observe in the absorption spectrum at 590 and 425 nm. Since the calculated oscillator strength is also very low, we do not expect this state to contribute to the observed absorption spectrum. According to the linear response calcula-

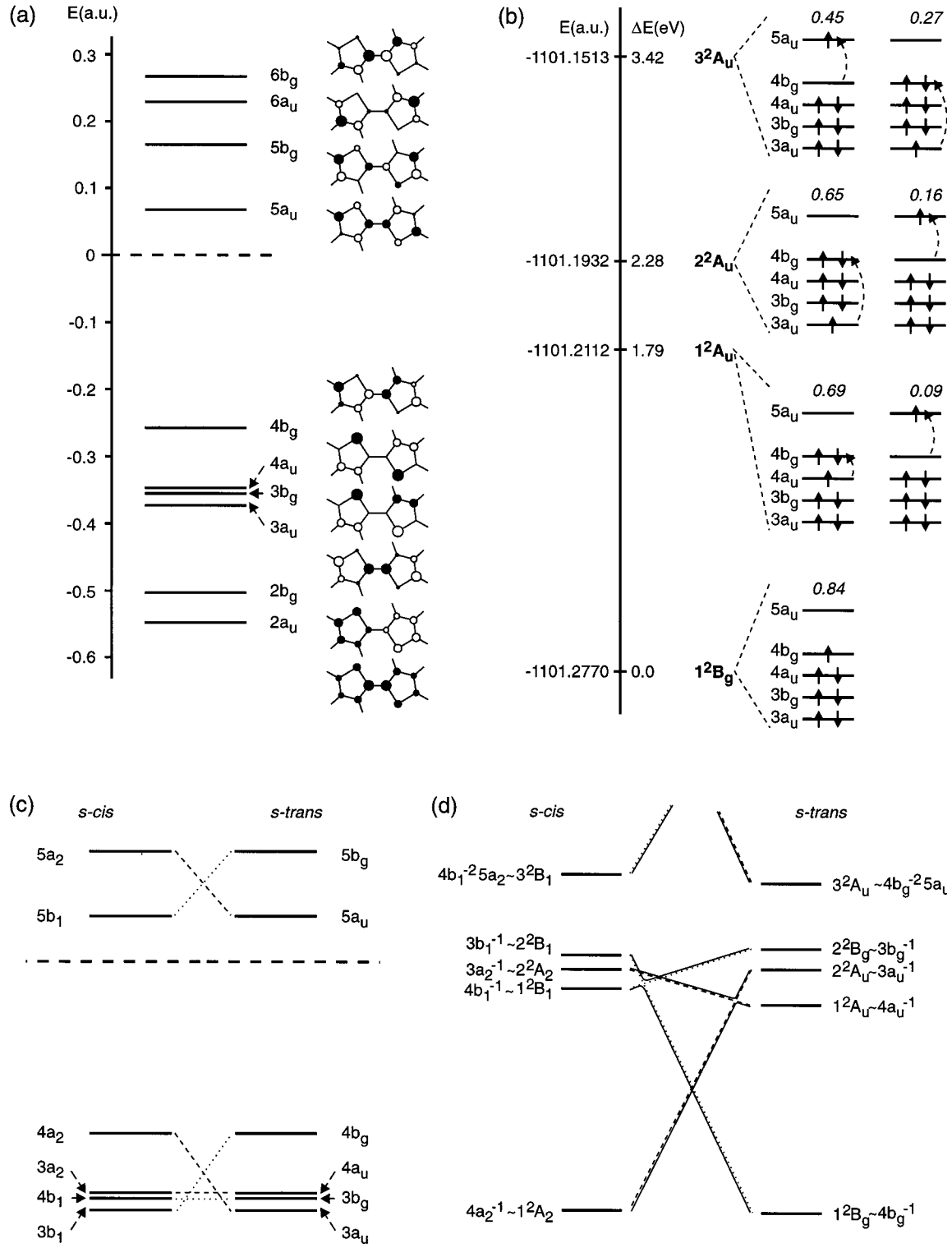

Figure 5. (a) Schematic diagram showing the RHF energies and atomic orbital compositions of the valence π-molecular orbitals of neutral *s-trans*-bithiophene, calculated at the planar geometry of the radical cation. (b) Orbital occupations and weights for the most important ($c_i^2 > 0.05$) electronic configurations in the CASSCF wave function for the ground 1^2B_g and the vertical excited 1^2A_u, 2^2A_u, and 3^2A_u states of the *s-trans*-bithiophene radical cation. Excitations are indicated by dashed arrows. Note that each electronic state is described by its own set of natural orbitals. (c) Valence π-orbital correlation diagram for the s-cis to s-trans interconversion of neutral bithiophene, with the C_2 axis as the symmetry element conserved during the interconversion. (d) Qualitative state correlation diagram for the s-cis to s-trans interconversion of the bithiophene radical cation with the C_2 axis as the symmetry element conserved during the interconversion, based on the orbital correlations in Figure 5c and the dominating configuration in each state according to CASSCF calculations.

tions, the next ^2A_u state lies at 2.05 eV (606 nm), and the oscillator strength for a transition to this state from the ground state is 0.191 in the length and 0.158 in the velocity representation, while the third ^2A_u excited state is at an energy of 2.77 eV (447 nm) with an oscillator strength of 0.356 (length) and 0.321 (velocity). Given the moderate basis set and active space used in our calculations, together with the calculated oscillator strengths and the spread between the calculated excitation energies, the calculated transition energies to these states are sufficiently close to the experimental ones to unambiguously

TABLE 2: Vertical Excitation Energies (in eV, cm^{-1}, and for Easier Comparison, in nm) and Oscillator Strengths in the Diplole Length and Dipole Velocity Representations from the CASSCF Linear Response Calculations for Excitations to the First Three Excited Doublet States of Each Symmetry from the 1^2B_g Ground State of s-trans and the 1^2A_2 Ground State of s-cis Bithiophene Radical Cation

excited state		energy			oscillator strength	
sym.	no.	eV	cm^{-1}	nm	length	velocity
		s-trans Rotamer				
A_u	1	1.75	14122	709	0.0032	0.0024
	2	2.05	16524	606	0.1906	0.1577
	3	2.77	22375	447	0.3564	0.3206
B_g	1	2.22	17966	557	dipole forbidden	
	2	4.11	33192	301	transitions	
	3	4.63	37356	268		
A_g	1	6.83	55117	182	dipole forbidden	
	2	7.06	57046	176	transitions	
	3	7.67	61958	162		
B_u	1	7.06	57010	176	0.0000	0.0005
	2	7.25	58536	171	0.0066	0.0085
	3	7.98	64479	155	0.0004	0.0000
		s-cis Rotamer				
B_1	1	1.85	14947	670	0.0249	0.0130
	2	2.17	17496	572	0.1770	0.1597
	3	2.83	22844	438	0.3152	0.2840
A_2	1	2.03	16433	609	0.0034	0.0045
	2	4.18	33774	296	0.0000	0.0001
	3	4.77	38517	260	0.0863	0.0645
A_1	1	6.62	53448	187	dipole forbidden	
	2	7.29	58907	170	transitions	
	3	7.75	62624	160		
B_2	1	6.95	56132	178	0.0002	0.0012
	2	7.18	57946	173	0.0003	0.0002
	3	7.71	62222	161	0.0036	0.0041

assign the observed 590 nm absorption band as the $1^2B_g \rightarrow 2^2A_u$ transition and the 425 nm band as the $1^2B_g \rightarrow 3^2A_u$ transition. The ratio of the calculated oscillator strengths of the high- and low-energy transitions is ~2:1, rather low compared to the experimental intensity ratio of approximately 5:1. In a similar fashion, the calculated 2.17 eV (572 nm) $1^2A_2 \rightarrow 2^2B_1$ and the 2.83 eV (438 nm) $1^2A_2 \rightarrow 3^2B_1$ transitions of the s-cis rotamer are identified as the transitions that might contribute to the observed absorption spectrum.

Vertical Excited States. Having identified the electronic transitions contributing to the experimental spectrum, we performed CASSCF calculations on the corresponding excited states at the two ground state optimized geometries: 2^2A_u, 3^2A_u for the s-trans and 2^2B_1, 3^2B_1 for the s-cis rotamer. For the sake of completeness, the 1^2A_u and 1^2B_1 states were also computed. The most important electronic configurations in a natural orbital basis contributing to these excited states and their weights in the CASSCF wave functions are shown for the s-trans rotamer in Figure 5b. (Since the CASSCF calculations do not yield orbital energies, the orbitals are given in the order they appear in the RHF wave function of neutral bithiophene). The 1^2B_g ground state of the s-trans rotamer is mainly described by the (s-trans 2T)$(4b_g)^{-1}$ configuration, which contributes 0.84 to the CASSCF wave function. As expected from qualitative considerations, mainly the $4a_u \rightarrow 4b_g$, $3a_u \rightarrow 4b_g$, and $4b_g \rightarrow 5a_u$ excitations contribute to the three lowest excited states of ^2A_u symmetry. All three states are described by two principal configurations each (configurations with weights grater than 0.05 are considered). The 1^2A_u state wave function contains the (s-trans 2T)$(4a_u)^{-1}$ and (s-trans 2T)$(4b_g)^{-2}(5a_u)^1$ configurations with respective weights of 0.69 and 0.09. The 2^2A_u state is described by the (s-trans 2T)$(3a_u)^{-1}$ and (s-trans 2T)$(4b_g)^{-2}(5a_u)^1$ configurations, with weights of 0.65 and 0.16, while the 3^2A_u state contains the same two main configurations with weights of 0.27 and 0.45, respectively. The vertical transition energies to these states are calculated to be 1.79, 2.28, and 3.42 eV. These should be compared with the 1.75, 2.05, and 2.77 eV values from the linear response calculations, and the 2.10 and 2.91 eV experimental ones. The linear response calculations underestimate the experimental transition energies by 2% and 5%, respectively, and the excitation energies from the independent CASSCF calculations on the vertical excited states are in error by 9% and 18%.

The $^2A_2$ ground state of the s-cis rotamer is described by the (s-cis 2T)$(4a_2)^{-1}$ configuration with a weight of 0.83. Similarly to the lowest three ^2A_u excited states of the s-trans rotamer, the corresponding $^2B_1$ states of the s-cis rotamer are described by two main configurations each. The main configurations contributing to the 1^2B_1 state are (s-cis 2T)$(4b_1)^{-1}$ (0.63) and (s-cis 2T)$(4a_2)^{-2}(5b_1)^1$ (0.15), to the 2^2B_1 state (s-cis 2T)$(3b_1)^{-1}$ (0.70) and (s-cis 2T)$(4a_2)^{-2}(5b_1)^1$ (0.09), and finally to the 3^2B_1 state (s-cis 2T)$(4a_2)^{-2}(5b_1)^1$ (0.46) and (s-cis 2T)$(3b_1)^{-1}$ (0.25) (weights in the CASSCF wave function are given in parentheses). The calculated vertical excitation energies are 1.99, 2.34, and 3.42 eV. The corresponding values from the linear response calculations are 1.85, 2.17, and 2.83 eV. We note that there is a very close correspondence between the electronic structure of these four states of the s-cis rotamer and the four states of the s-trans rotamer discussed in the previous paragraph.

Figure 5c shows the valence π-orbital correlation diagram for the s-cis to s-trans interconversion of neutral bithiophene, with the C_2 axis as the symmetry element conserved during the interconversion. Figure 5d shows a qualitative state correlation diagram for the s-cis to s-trans interconversion of the bithiophene radical cation (once more with the C_2 axis as the symmetry element conserved), based on these orbital correlations and the dominating configuration in each state according to the CASSCF calculations (see Figure 5b for the s-trans rotamer; the s-cis states are very similar with appropriate orbital substitutions).

Excited State Geometries of the Radical Cation. Having obtained converged CASSCF wave functions for the vertical excited states, we calculated the Hessian matrices ("vertical Hessian") and carried out CASSCF geometry optimizations of the lowest three ^2A_u excited states of the s-trans rotamer in C_{2h} symmetry, and of the 2^2B_1 and 3^2B_1 excited states of the s-cis rotamer in C_{2v} symmetry. The vertical Hessian matrix is positive definite for the 1^2A_u state, while the matrix has one negative eigenvalue for the 2^2A_u, 3^2A_u, 2^2B_1, and 3^2B_1 states. At the optimized geometries of the excited states, also the Hessian matrix ("adiabatic Hessian") for the 3^2A_u state has become positive definite. Optimization of the 1^2A_u and 3^2A_u states thus leads to real minima, while the optimized C_{2v} structure of the 2^2B_1 and 3^2B_1 s-cis states both have one normal mode of a_2 symmetry with an imaginary frequency, and the optimized C_{2h} structure of the 2^2A_u s-trans state has one normal mode of a_u symmetry with an imaginary frequency of 40.2i cm^{-1}. This indicates that the real minima of the 2^2A_u, 2^2B_1, and 3^2B_1 states have C_2 symmetry, or lower. Optimization in these point groups was however not attempted. For the s-trans rotamer, the calculated adiabatic energies are 1.48, 2.16, and 3.33 eV. Thus, at the C_{2h} optimized structures, the three lowest ^2A_u excited states are 0.31, 0.12, and 0.09 eV lower in energy than at the ground state geometry. The optimized geometrical parameters are given in Table 3, where they are compared to those of the ^2B_g ground state. The structures of the radical cation in the three excited states are very different, and this can be rationalized qualitatively from the electronic structures of the excited states

TABLE 3: Calculated Geometrical Parameters of the s-trans Rotamer of the Bithiophene Radical Cation in the Ground and the First Three ^2A_u Excited States: CASSCF/6-31G* Optimized Geometries and Extrapolated Equilibrium Geometries from the Vertical Hessian Approach (See Text for Details) (Bond Lengths in Ångströms, Bond Angles in Degrees)

	1^2B_g	1^2A_u		2^2A_u		3^2A_u	
s-trans	CASSCF	CASSCF	extrap.	CASSCF	extrap.	CASSCF	extrap.
$r_{22'}$	1.399	1.440	1.547	1.451	1.447	1.421	1.421
r_{12}	1.737	1.720	1.834	1.746	1.750	1.773	1.771
r_{15}	1.708	1.740	1.612	1.720	1.716	1.708	1.707
r_{45}	1.392	1.357	1.297	1.415	1.415	1.408	1.408
r_{34}	1.389	1.452	1.609	1.398	1.399	1.388	1.388
r_{23}	1.421	1.385	1.139	1.398	1.392	1.437	1.436
$\alpha_{122'}$	122.7	120.6	117.9	121.9	121.9	120.5	120.5
α_{215}	91.6	93.0	95.8	91.5	91.4	90.8	90.8
α_{154}	112.9	111.1	109.5	111.7	111.7	113.6	113.6
α_{345}	112.2	112.6	112.6	112.6	112.6	112.8	112.8
α_{234}	113.0	112.7	113.3	112.7	112.8	112.2	112.2
α_{123}	110.3	110.5	108.9	111.5	111.5	110.6	110.6

discussed above and displayed in Figure 5b. The 1^2A_u excited state is dominated by the (s-trans 2T)$(4a_u)^{-1}$ configuration, and $4a_u$ is mostly a nonbonding orbital, with bonding character only between C_3 and C_4. The geometrical changes in bond lengths upon the $1^2B_g \rightarrow 1^2A_u$ adiabatic transition are the opposite of those observed upon ionization of 2T and are qualitatively explained by differences in bonding character of the $4a_u$ and $4b_g$ orbitals. The minimum energy structure in the 1^2A_u state is in fact quite similar to that of neutral bithiophene, with the exception of the $S_1-C_2-C_{2'}-S_{1'}$ dihedral angle, since the radical cation excited state is planar. On the other hand, the changes in geometry between the 1^2B_g and the 3^2A_u states are in the same direction as the ones upon going from the neutral to the radical cation (i.e., elongation of the C_2-C_3, C_4-C_5, and S_1-C_2 bonds, shortening of the $C_2-C_{2'}$, C_3-C_4, and S_1-C_5 bonds), with the exception of the $C_2-C_{2'}$ bond which is getting longer in the excited state. Except for the $C_2-C_{2'}$ elongation, these changes are qualitatively described by the removal of two electrons from the $4b_g$ orbital and addition of one electron to the $5a_u$ orbital relative to neutral 2T with 45% weight, and removal of one electron from $3a_u$ with 27% weight. The two configurations have the opposite effect on the $C_2-C_{2'}$ bond length, and qualitative molecular orbital theory can therefore only say that the elongation is not in contradiction with the orbital picture, but it explains why the $C_2-C_{2'}$ bond is shorter for 3^2A_u than for 2^2A_u. (We note that the excited states are intrinsically multiconfigurational, and thus the results cannot be interpreted in a single configuration picture.) The individual thiophene rings thus have a quinoid-like structure for the for 3^2A_u state, with a relatively long C−C bond connecting them. We note here that this structure is different from the fully quinoid structure of the bithiophene dication,[9c] where the rings are connected by a short C−C bond. As noted above, the optimized C_{2h} structure of the 2^2A_u state is not a real minimum. The largest geometry change is the elongation of the $C_2-C_{2'}$ bond by 0.052 Å and the second largest change is the shortening of the C_2-C_3 bond by 0.033 Å, both changes in agreement with the differences in bonding character of the $4b_g$ orbital and the $3a_u$ and $5a_u$ orbitals.

Calculated Ground State Vibrational Frequencies and Normal Modes. Previously, we employed unscaled UB-LYP/6-31G* calculated vibrational frequencies to assign the resonance Raman spectrum of the bithiophene radical cation.[11] Having obtained optimized geometries of both the s-trans and the s-cis rotamers in the ground state, using also the UB3-LYP and CASSCF methods (see Table 1), we compare the vibrational frequencies calculated at these geometries with the experimental data. The calculated vibrational wavenumbers of the $\nu_4-\nu_{15}$ totally symmetric (a_g) fundamentals of the s-trans rotamer were fitted to the corresponding experimentally observed values, using a single multiplicative scaling factor. The root-mean-square deviation between the experimental and unscaled calculated wavenumbers of these 12 fundamentals is 23.1 cm^{-1} for UB-LYP, 28.9 cm^{-1} for UB3-LYP, and 102.3 cm^{-1} for CASSCF. It should be noted here that since the active space for the CASSCF calculations only contains the valence-π orbitals, the vibrational normal modes involving the σ-backbone alone are effectively described at the HF level. The UB-LYP method generally underestimates the vibrational frequencies, while the hybrid UB3-LYP and the CASSCF methods overestimate those. This is also evident from the scaling factors we obtain, their values being 1.0132 for UB-LYP, 0.9766 for UB3-LYP, and 0.9131 for CASSCF. Employing these scaling factors leads in all three cases to an improvement of the agreement between the experimental and scaled calculated frequencies. The largest improvement is for the CASSCF frequencies, the root-mean-square deviation between the experimental and scaled wavenumbers decreases to 9.6 cm^{-1}, the largest absolute deviation being 20.2 cm^{-1}. In terms of scaled frequencies, the rms deviation is 13.3 cm^{-1} for UB3-LYP and 18.5 cm^{-1} for UB-LYP, with largest absolute deviations of 20.7 and 27.1 cm^{-1}, respectively.

A complete normal coordinate analysis in terms of internal coordinates or internal symmetry coordinates is beyond the scope of this article. Nevertheless, visual inspection of the normal modes is important for characterizing the molecular motions associated with the experimental Raman bands. The CASSCF calculated $\nu_4-\nu_{15}$ normal modes of the s-trans rotamer, corresponding to the experimentally observed bands, are therefore shown in Figure 6. The normal modes calculated by the UB-LYP and UB3-LYP methods are very similar to the CASSCF calculated ones.

Assignment of the Vibrational Spectrum. In our previous communication, we have presented and assigned the resonance Raman spectrum, measured using 425 nm excitation, of the photochemically generated bithiophene radical cation in the 275−1600 cm^{-1} wavenumber region.[11] Here, we present the 425 nm excited resonance Raman spectrum of the bithiophene radical cation generated radiolytically in a glassy matrix in the 275−2300 cm^{-1} wavenumber range (see Figure 3).

As seen from Figure 2, the 425 nm excited Raman spectra obtained in solution (trace c) and in the Freon glass (trace b) are quite similar, nevertheless small differences, on the order of 2−5 cm^{-1}, are observed between the experimental band positions in the two media. As in the case of the solution spectrum, we assign the matrix spectrum to the more stable s-trans rotamer of the bithiophene radical cation, with only one band, at 640 cm^{-1}, attributed to the s-cis rotamer. This band was assigned to the higher energy s-cis rotamer on the basis of the different intensities, relative to the other bands, observed in the room-temperature solution and the low-temperature matrix experiments.[11] This assignment is supported by the computational results presented below. The assignment of the low-temperature matrix Raman spectrum between 275 and 1600 cm^{-1} is not much different from that of the room-temperature solution spectrum. One difference is the observation of the ν_{14} fundamental at 378 cm^{-1}, which has not been seen in the solution spectrum. The other is that due to the somewhat smaller line widths in the low-temperature spectra, the shoulder on the high-wavenumber side of the ν_4 band (1532 cm^{-1} in solution,

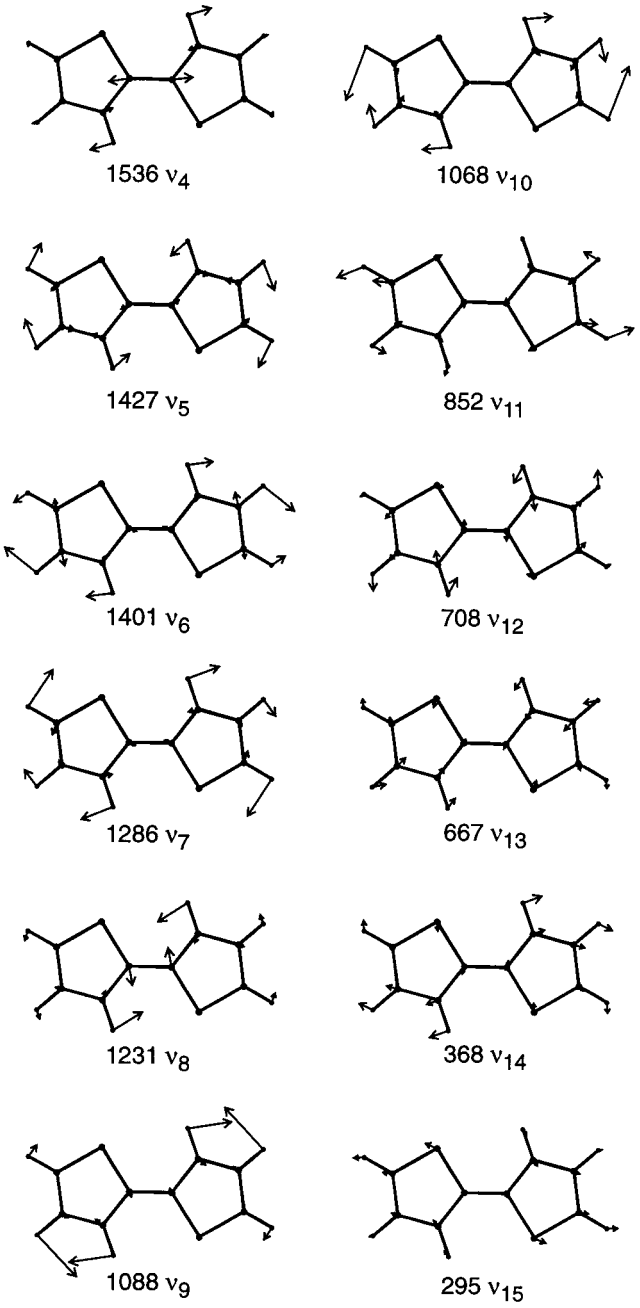

Figure 6. Totally symmetric (a_g) normal modes of vibration of the s-trans rotamer of the bithiophene radical cation, corresponding to the fundamentals observed in the resonance Raman spectrum (scaled CASSCF wavenumbers).

1535 cm^{-1} in the Freon matrix) clearly manifests itself as a band at 1551 cm^{-1}, and is assigned as the $\nu_{11} + \nu_{13}$ combination. In the 1600−2300 cm^{-1} region, a number of combination and overtone bands are observed, mainly involving the ν_{13} fundamental. In the whole spectrum, numerous bands are identified as combinations or overtones involving the ν_{13} fundamental: the first and second overtones at 1358 and 2034 cm^{-1}, respectively, combinations with the ν_{15} (979 cm^{-1}), ν_{12} (1393 cm^{-1}), ν_{11} (1551 cm^{-1}), ν_{10} (1747 cm^{-1}), ν_8 (1896 cm^{-1}), ν_7 (1953 cm^{-1}), ν_6 (2068 cm^{-1}), ν_5 (2114 cm^{-1}), and ν_4 (2213 cm^{-1}) fundamentals (positions of the combination bands in parentheses), and finally two combinations involving the first overtone of ν_{13}, namely $\nu_{15} + 2\times\nu_{13}$ at 1656 cm^{-1} and $\nu_{11} + 2\times\nu_{13}$ at 2229 cm^{-1}. Apart from $2\times\nu_{13}$ (1358 cm^{-1}), first overtones of ν_{15} (600 cm^{-1}), of ν_{12} (1435 cm^{-1}), and possibly of ν_{11} (1747 cm^{-1}) are identified. The complete assignment of the resonance Raman spectrum is given in Figure 3 and Table 4.

TABLE 4: Experimental and Scaled[a] Calculated Vibrational Frequencies (cm^{-1}) of the Totally Symmetric Modes of the Bithiophene Radical Cation and Assignments[b] of the Overtone and Combination Bands of the s-trans Rotamer

normal mode	s-trans				s-cis			
	exptl	BLYP	B3LYP	CAS	exptl	BLYP	B3LYP	CAS
1		3228	3193	3149		3229	3193	3150
2		3212	3179	3134		3217	3185	3145
3		3195	3161	3120		3206	3173	3129
4	1535	1515	1523	1536		1510	1520	1536
5	1435	1458	1450	1427		1449	1440	1416
6	1393	1408	1406	1401		1406	1405	1400
7	1276	1291	1287	1286		1291	1285	1284
8	1219	1196	1205	1231		1158	1154	1156
9	1083	1097	1092	1088		1091	1085	1072
10	1070	1088	1082	1068		1065	1067	1063
11	872	853	856	852		850	852	848
12	715	688	694	708		695	699	708
13	678	662	666	667	640	609	619	631
14	378	377	374	368		322	323	324
15	300	284	287	295		134	134	140

overtones and combinations	assignment (s-trans)	overtones and combinations	assignment (s-trans)
2259	$\nu_6 + \nu_{11}$(?)	1656	$\nu_{15} + 2\times\nu_{13}$
2229	$\nu_{11} + 2\times\nu_{13}$	1551	$\nu_{11} + \nu_{13}$
2213	$\nu_4 + \nu_{13}$	1435	$2\times\nu_{12}$
2145	$\nu_7 + \nu_{11}$(?)	1393	$\nu_{12} + \nu_{13}$
2114	$\nu_5 + \nu_{13}$	1358	$2\times\nu_{13}$
2068	$\nu_6 + \nu_{13}$	1166	$2\times\nu_{42} + \nu_{13}$ (?)
2034	$3\times\nu_{13}$	979	$\nu_{15} + \nu_{13}/4\times\nu_{42}$ (b_g) (?)
1953	$\nu_7 + \nu_{13}$	600	$2\times\nu_{15}$
1896	$\nu_8 + \nu_{13}$	488	$2\times\nu_{42}$ (b_g) (?)
1747	$\nu_{10} + \nu_{13}/2\times\nu_{11}$		

[a] The following scaling factors were used: 1.0132 for B-LYP, 0.9766 for B3-LYP, and 0.9131 for CASSCF. [b] Question marks denote tentative assignments.

In our previous communication,[11] we assigned the 488 cm^{-1} band (491 cm^{-1} in the solution spectrum) to the first overtone of the ν_{42} fundamental of b_g symmetry and noted that the presence of an overtone of a nontotally symmetric mode implies that the radical cation is nonplanar in the resonant excited state. Our CASSCF calculations on the other hand predict that the equilibrium structure of the radical cation in the 3^2A_u state is planar. However, the vertical Hessian matrix has one negative eigenvalue for the 3^2A_u state, which might explain how the $2\times\nu_{42}$ mode can gain intensity. At present we believe that the assignments involving $2\times\nu_{42}$ should be labeled as tentative.

Calculation of the Absorption Spectrum and Resonance Raman Intensities. The detailed formalism of the theoretical treatment has been discussed previously.[22a] Here, only a qualitative description shall be given.

The theoretical calculation of optical absorption spectra and resonance Raman intensities is usually performed using the Born−Oppenheimer and Condon approximations assuming resonance with a single electronic transition. The present work does not go beyond these approximations. Moreover, the potentials are assumed to be harmonic and multidimensional over the region of interest. We shall here use the wave packet propagation formalism developed by Heller and co-workers.[23] The electronic absorption band shape and the resonance Raman intensity depend on the time-dependent overlaps (autocorrelators) $\langle i|i(t)\rangle$ and $\langle f|i(t)\rangle$, respectively, where $\langle i|$ is the initial state in the absorption and Raman process and $\langle f|$ is the final state in the resonance Raman process. The time dependence of $|i(t)\rangle$

represents the motion of the nuclei under the influence of the upper state potential after an instantaneous excitation from the lower to the upper electronic state. In the present work, the evaluation of autocorrelators is performed by use of recursion formulas given in ref 24. The absorption spectrum is then given by the full Fourier transform of the overlap of this time-dependent wave packet with itself at time zero, while the resonance Raman cross section is obtained from the half Fourier integral of the overlap of the evolving wave packet with that of the final state. The vibrational Hamiltonians of the lower and upper states are written in terms of dimensionless normal coordinates. The potential surfaces are each characterized by a set of normal coordinates and vibrational frequencies, while their relative positions are described by the Duschinsky rotation matrix and a set of dimensionless displacements. In the following, the parameters which characterize the potential surfaces and their relative positions are referred to as the *vibrational parameters*. These quantities are derived from the harmonic force fields (Hessian matrices) of the electronic ground and excited states, obtained from our CASSCF quantum chemical calculations. We use two different approaches for the determination of the vibrational parameters, denoted as the *adiabatic approach* and the *vertical approach*.[22]

In the *adiabatic approach*, optimizations of both the ground and excited-state geometries are carried out, and the Hessian matrices of both states are calculated at the optimized geometries. In other words, the potential surfaces are expanded around different points, namely the optimized geometries of the respective electronic states. From the Cartesian displacements between the ground and excited electronic states, the dimensionless displacements and the Duschinsky rotation matrix are calculated, using expressions given by Warshel and Karplus.[25] In this case, the dimensionless displacements are essentially the projections of the Cartesian displacement vectors onto the ground state normal modes. The vibrational parameters obtained in this way are then used as input parameters for the evaluation of optical absorption spectra and resonance Raman intensities by means of the wave packet propagation techniques described above.

In the *vertical approach*, the ground and excited state potential energy surfaces are expanded to second order in the nuclear coordinates around the same point, the equilibrium geometry of the ground electronic state. Two degrees of sophistication are used within the vertical approach, the *vertical Hessian* and the *vertical gradient* approaches. In the *vertical Hessian approach*, the ground state geometry is optimized, and at this geometry, both the ground and the excited state Hessians are evaluated, together with the gradient on the excited state surface. From the gradient and Hessian of the excited state the geometry change upon excitation can be determined provided that the harmonic approximation is valid in a sufficiently large neighborhood of the ground state geometry. Having determined the geometry change upon excitation, the dimensionless displacements and the Duschinsky rotation matrix are calculated in the same way as in the adiabatic approach. These parameters are used to calculate optical absorption and Raman spectra. The *vertical gradient approach* is more crude, it differs form the vertical Hessian approach in that in the excited state only the gradient is directly calculated, while the Hessian is not calculated but assumed to be identical to that of the ground state.

In the procedure of calculating absorption spectra, the transition energy at equilibrium, E_0, and a homogeneous damping factor (or bandwidth, which is inversely proportional to the lifetime of the excited state), Γ, are used as fitting parameters to obtain the best agreement with the observed absorption spectrum. Their values derived in this way are then used together with the vibrational parameters in the calculation of the resonance Raman spectra. In the calculation of the resonance Raman spectra only totally symmetric fundamentals and their first overtones are considered. The vibrational parameters are obtained from unscaled CASSCF Hessians both in the adiabatic and the vertical methods. The calculated resonance Raman spectra are, however, *plotted* using the scaled CASSCF frequencies listed in the fifth column of Table 4.

Instead of carrying out a full time-domain calculation, a crude estimate of relative resonance Raman intensities can be obtained by use of the *Savin formula*,[23b,26] which states that the resonance Raman intensity is proportional to $\Delta_i^2\omega_i^2$, where ω_i is the angular frequency for mode i of the ground electronic state, and Δ_i is the dimensionless displacement calculated by either the *adiabatic* or one of the two *vertical* approaches. This formula is only valid under the condition that the absorption spectrum is broad and unstructured and its width is large compared to ω_i. In the situation of structured absorption bands, the Savin formula is applicable for a comparison of the intensities of close lying Raman bands only.

For large polyatomic molecules with many vibrational degrees of freedom and/or large damping factors, the absorption spectrum is often broad and unstructured. In such situations, optical absorption and resonance Raman spectroscopy only probe the excited-state potential energy surface in the neighborhood of the Franck−Condon region. Thus, in these cases the vertical approach provides a better approximation to the excited state potential energy surface. On the other hand, for small polyatomic molecules which often have structured absorption bands, implying long excited state lifetimes, the adiabatic approach may yield the best result because the wave packet now samples information in a large region of the excited potential surface centered around the equilibrium geometry of the excited electronic state.

When the adiabatic approach gives good agreement between the calculated and observed absorption and resonance Raman spectra, it is an indication that the optimized excited state equilibrium geometry is close to the experimental one. In the vertical approach, the geometry change upon excitation is derived from the gradient and Hessian of the excited state, and thus an *extrapolated* excited state geometry can be calculated. When determining the excited-state geometry this way, it is assumed that the excited state potential energy surface is well described by a harmonic approximation in the region between the vertical geometry and the extrapolated one. In fact, if the extrapolated and optimized excited state geometries are similar, this indicates that the potential energy surface is reasonably well described by a harmonic potential. On the other hand, considerable differences of the two geometries can be taken as an indication of substantial anharmonicity along the path from one geometry to the other.

The bithiophene radical cation is a medium sized polyatomic molecule, its absorption spectrum shows a structured, intense band (425 nm), and a broad unstructured band of lower intensity (590 nm). It is thus interesting to compare the performance of the adiabatic and vertical approaches from a methodological point of view, and also as a measure of possible anharmonicity in the excited states. (We have previously discussed the case of the *N*,*N*′-dimethylpiperazine radical cation,[22] where strong anharmonicity of the excited state surface was observed.) In the following, the results of our calculations of the optical absorption bands and resonance Raman intensities will be

TABLE 5: Calculated Excited State Wavenumbers (Unscaled CASSCF, in cm^{-1}) and Dimensionless Displacements for the $1^2B_g \rightarrow 2^2A_u$ and $1^2B_g \rightarrow 3^2A_u$ Transitions of s-trans Bithiophene Radical Cation

	vertical gradient		vertical Hessian		adiabatic	
	waven.	displ.	waven.	displ.	waven.	displ.
			$1^2B_g \rightarrow 2^2A_u$			
1	3448	−0.04516	3447	−0.04133	3457	−0.04218
2	3433	0.00140	3434	0.00586	3435	0.00467
3	3417	0.00216	3415	−0.00190	3418	0.00039
4	1682	0.81050	1974	0.79847	2310	0.77893
5	1563	−0.00694	1622	−0.15771	1593	−0.18279
6	1535	0.18066	1491	0.13894	1467	0.10202
7	1409	0.13080	1457	0.22801	1409	0.26641
8	1348	−0.38773	1401	−0.22334	1350	−0.11714
9	1191	0.12561	1218	0.06169	1193	0.07733
10	1169	0.49113	1183	0.43242	1137	0.43063
11	933	−0.51473	938	−0.53390	928	−0.55400
12	775	−0.37073	802	−0.14882	823	−0.08358
13	731	0.19511	739	0.00902	733	−0.09411
14	403	0.09395	401	0.09672	391	−0.02970
15	324	0.82708	324	0.71120	318	0.69619
			$1^2B_g \rightarrow 3^2A_u$			
1	3448	−0.01834	3449	−0.01669	3449	−0.01852
2	3433	−0.01549	3432	−0.01496	3435	−0.01666
3	3417	0.01885	3413	0.01730	3422	0.01714
4	1682	−0.01990	1968	0.06691	1913	0.06149
5	1563	−0.11047	1563	−0.12028	1547	−0.12518
6	1535	0.15261	1546	0.07317	1537	0.07303
7	1409	0.22579	1412	0.19046	1397	0.19392
8	1348	−0.01409	1362	−0.01683	1304	−0.01785
9	1191	−0.13043	1206	−0.07307	1203	−0.07751
10	1169	0.28770	1168	0.24638	1151	0.25163
11	933	−0.16807	936	−0.18367	935	−0.19885
12	775	−0.83769	804	−0.71023	794	−0.73015
13	731	−0.98222	728	−0.92812	712	−0.97081
14	403	−0.23943	413	−0.32137	406	−0.32523
15	324	0.43826	311	0.45451	302	0.52658

discussed separately for the two electronic transitions ($1^2B_g \rightarrow 2^2A_u$ and $1^2B_g \rightarrow 3^2A_u$) of the s-trans and for the $1^2A_2 \rightarrow 3^2B_1$ transition of the s-cis rotamer of the bithiophene radical cation.

Calculations on the s-trans Rotamer. First, we consider the 590 nm absorption band and the corresponding Raman spectrum. Since our calculations identified the excited state of this transition as the 2^2A_u state, the necessary excited state vibrational parameters have been obtained from CASSCF calculations on this state. The CASSCF calculated vibrational frequencies and the corresponding dimensionless displacements are given for the vertical gradient, vertical Hessian, and adiabatic approaches in the upper half of Table 5. Since the same molecular point group was used in the two states, only the totally symmetric (a_g) modes $\nu_1-\nu_{15}$ have nonzero displacements. From Table 5, it is seen that there are substantial differences between the displacements calculated by the different approaches, even though they are in agreement on assigning the largest displacements to the ν_4, ν_{10}, ν_{11}, and ν_{15} modes. The upper panel of Figure 7 shows the absorption spectra calculated by the vertical Hessian (trace ii) and the adiabatic (trace iii) methods, compared to the experimental spectrum (trace i). The calculated spectra have been obtained using $E_0 = 16500$ cm^{-1} (2.05 eV) and $\Gamma = 500$ cm^{-1} for the vertical Hessian case, and $E_0 = 15800$ cm^{-1} (1.96 eV) and $\Gamma = 500$ cm^{-1} for the adiabatic one. They differ from the experimental spectrum in that apart from the main peak at 16950 cm^{-1} there is an additional one at 18300 cm^{-1} in the vertical Hessian spectrum, and a shoulder at ~18000 cm^{-1} in the adiabatic spectrum. On the whole, however, both methods give a qualitatively correct picture of the absorption band, with the adiabatic approach performing slightly better. The lower

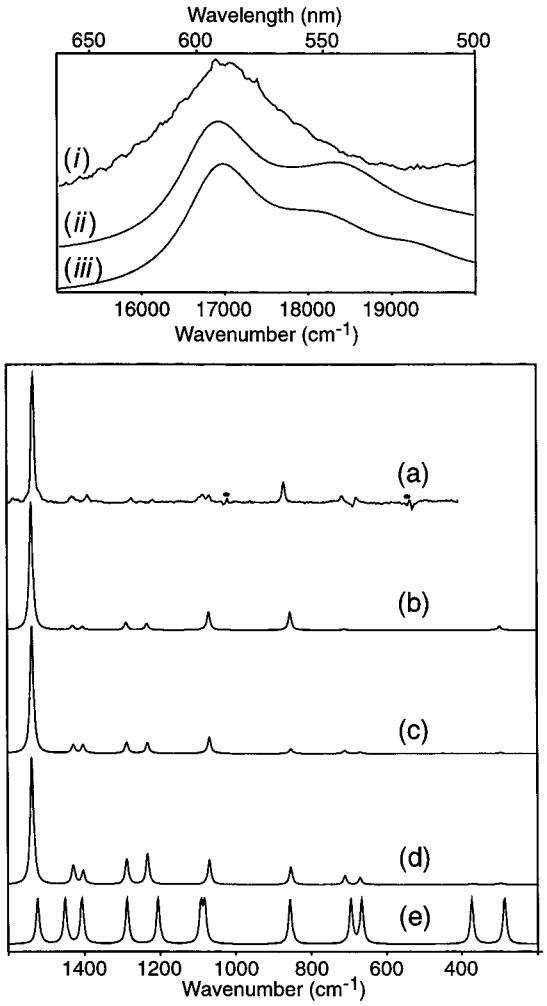

Figure 7. (upper window) Experimental and simulated electronic absorption spectra of s-trans $2T^{+\bullet}$ in the 15000−20000 cm^{-1} wavenumber range (667−500 nm): (i) experimental spectrum; (ii) calculated spectrum vertical Hessian approach ($E_0 = 16500$ cm^{-1}, $\Gamma = 500$ cm^{-1}); (iii) calculated spectrum adiabatic approach ($E_0 = 15800$ cm^{-1}, $\Gamma = 500$ cm^{-1}). (lower window) Experimental and simulated 550 nm excited resonance Raman spectra of $2T^{+\bullet}$ in the 1600−200 cm^{-1} wavenumber range: (a) experimental spectrum; (b) calculated spectrum vertical Hessian approach using the Savin formula; (c) calculated spectrum vertical Hessian approach full time-domain calculation; (d) calculated spectrum adiabatic approach; (e) UB3-LYP calculated spectrum with uniform band intensities.

panel of Figure 7 shows the calculated resonance Raman spectra for excitation at 550 nm. Comparing the Raman spectra from the full time-dependent calculations within the vertical Hessian (trace c) and adiabatic (trace d) methods, we can again see that both methods give a reasonable qualitative description of the experimental spectrum. The vertical Hessian method is mainly in error by predicting too low intensity for the ν_{11} mode (experimental wavenumber 872 cm^{-1}), while the adiabatic method underestimates the intensity of the ν_4 mode (1535 cm^{-1}) and overestimates that of the ν_7 (1276 cm^{-1}) and ν_8 (1219 cm^{-1}) modes. It is also interesting to investigate how the intensities predicted by the simple Savin formula compare to the experimental ones and to the ones given by the wave packet propagation calculations. A spectrum calculated by the vertical Hessian approach using the Savin formula is shown in trace b of Figure 7. Comparing it to the spectrum in trace c (vertical Hessian approach, full time domain calculation), the main difference is between the calculated intensity of the ν_{11} mode, the Savin formula giving higher intensity and thus better

agreement with experiment. We can conclude that both the adiabatic and the vertical Hessian methods (and in the latter case also the Savin formula) give qualitatively correct results, probably within the experimental errors of the resonance Raman intensities. The good performance of the Savin formula is in agreement with the fact that the 590 nm absorption band is unstructured and rather broad. The fact that the calculated spectra based on the vibrational parameters of the 2^2A_u electronic state are in agreement with the observed spectrum can be taken as further indication that the 550 nm excited resonance Raman spectrum should be considered dominantly resonant with the 590 nm absorption band.

For the 425 nm absorption band and the corresponding resonance Raman spectrum, the vibrational parameters were obtained from CASSCF calculations on the 3^2A_u state. The calculated vibrational frequencies and dimensionless displacements are given in the lower half of Table 5. There is considerably better agreement between the displacements, and also the vibrational frequencies, calculated by the different approaches than in the case of the $1^2B_g \rightarrow 2^2A_u$ transition. The vertical Hessian and adiabatic methods give almost identical displacements, and these differ substantially from those predicted by the vertical gradient method only in the case of the ν_4, ν_6, and ν_9 modes. The calculated absorption spectra are compared to the experimental spectrum in the upper panel of Figure 8. The spectrum shown in trace ii has been calculated by the vertical Hessian, while the one in trace iii by the adiabatic method. The calculated spectra have been obtained using $E_0 =$ 24000 cm^{-1} (2.98 eV) and $\Gamma = 100$ cm^{-1} for the vertical Hessian, and $E_0 = 24100$ cm^{-1} (2.99 eV) and $\Gamma = 100$ cm^{-1} for the adiabatic case. The two spectra are almost indistinguishable, which could be expected from the close agreement between the calculated displacements and frequencies and are in good agreement with the experimental one (trace i). The vibronic peaks are somewhat further apart in the calculated spectra than in the experimental one, this is due to the fact that, as noted above, for the calculation of the absorption spectrum unscaled CASSCF Hessians were used. As described before, a scaling factor of 0.9131 was found for the CASSCF frequencies, and applying the square of this factor (i.e., 0.8338) to the Hessian would decrease the spacing between the vibronic peaks thereby improving the agreement between experiment and calculation. The lower panel of Figure 8 shows the calculated Raman spectra for 425 nm excitation. As in the case of the absorption spectrum, the vertical Hessian (trace c) and adiabatic (trace d) methods give virtually identical spectra. The main difference between the calculated and the experimental (trace a) spectra is that the former predict too high intensity for the ν_{12} mode (experimental wavenumber 715 cm^{-1}) and its first overtone (1435 cm^{-1}, coinciding with the ν_5 mode in the experimental spectrum), and to a lesser extent also to the ν_{14} (378 cm^{-1}) and ν_{15} (300 cm^{-1}) modes. The intensity of the ν_4 mode (1535 cm^{-1}) is on the other hand somewhat underestimated. Nevertheless, just as in the case of the 550 nm excited Raman spectrum, we can conclude that the results given by both the adiabatic and the vertical Hessian methods are qualitatively correct, and, with the exception of the grossly overestimated intensity of the ν_{12} mode, probably within the experimental errors. The agreement between the spectrum calculated by the Savin formula (trace b) and the experimental one (trace a) is also in fair, but clearly poorer than in the case of the ones calculated by the vertical Hessian (trace c) and adiabatic (trace d) methods, as it is expected for a structured absorption band.

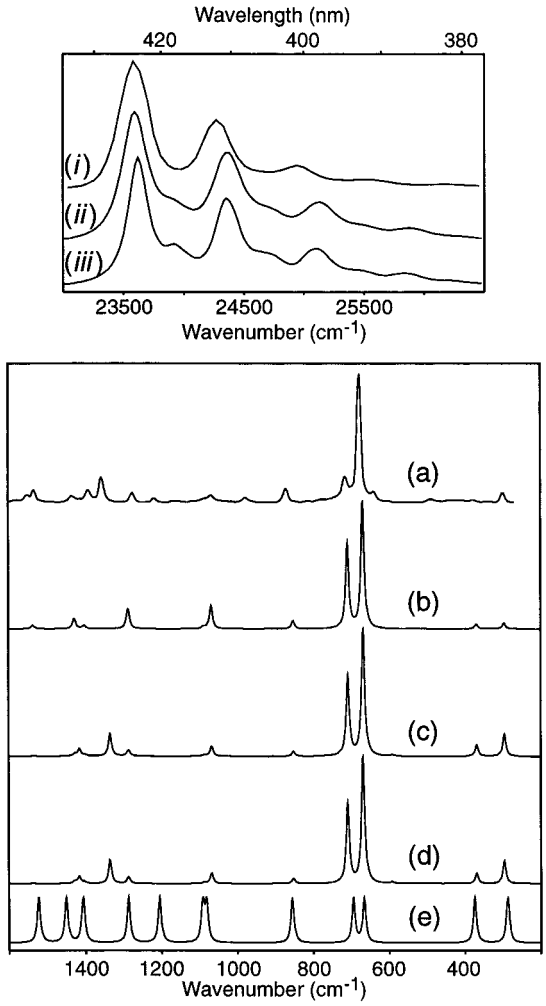

Figure 8. (upper window) Experimental and simulated electronic absorption spectra of s-trans $2T^{+\bullet}$ in the 23000−26500 cm^{-1} wavenumber range (435−377 nm): (i) experimental spectrum; (ii) calculated spectrum vertical Hessian approach ($E_0 = 24000$ cm^{-1}, $\Gamma = 100$ cm^{-1}); (iii) calculated spectrum adiabatic approach ($E_0 = 24100$ cm^{-1}, $\Gamma =$ 100 cm^{-1}). (lower window) Experimental and simulated 425 nm excited resonance Raman spectra of $2T^{+\bullet}$ in the 1600−200 cm^{-1} wavenumber range: (a) experimental spectrum; (b) calculated spectrum vertical Hessian approach using the Savin formula; (c) calculated spectrum vertical Hessian approach full time-domain calculation; (d) calculated spectrum adiabatic approach; (e) UB3-LYP calculated spectrum with uniform band intensities.

From the vertical Hessian calculations, we have obtained extrapolated equilibrium geometries for the three lowest ^2A_u excited states, assuming harmonic potentials. These are listed in Table 3, where they can be compared to the optimized (adiabatic) equilibrium geometries. In the case of the 1^2A_u state, the two geometries are very dissimilar, the differences in C−C and C−S bond lengths between the two geometries are in the 0.05−0.25 Å range. Even though we do not have experimental data for this state, and thus cannot directly assess the performances of the adiabatic and vertical approaches, the large discrepancy of the adiabatic and extrapolated geometries alone indicates substantial anharmonicity of the excited state potential. In the case of the 2^2A_u state, the largest differences between the two geometries are much smaller, 0.004 Å in bond lengths and 0.1° in the bond angles. The energy difference is also very small, the extrapolated geometry is 0.006 eV higher in energy than the adiabatic one. The adiabatic and extrapolated geometries of the 3^2A_u state are even more similar, the largest differences in bond lengths are 0.002 Å, while all bond angles are identical.

The energy difference is about 0.2 meV. These data are in accordance with the observation that the absorption and resonance Raman spectra calculated by the adiabatic and vertical Hessian methods are rather similar for the 2^2A_u state and very similar for the 3^2A_u state. We can thus conclude that the potential energy surface of the 2^2A_u state of the s-trans bithiophene radical cation is rather well described, and that of the 3^2A_u state is well described by a harmonic potential in the region between the vertical geometry of the 1^2B_g ground state and their respective optimized adiabatic equilibrium geometries.

The autocorrelators from which the absorption spectra are calculated in the vertical Hessian approach have a typical damping time of ~500 fs, both for the $1^2B_g \rightarrow 2^2A_u$ and for the $1^2B_g \rightarrow 3^2A_u$ transition. This is 10−20 times longer than the vibrational periods of the modes observed with highest intensity. Consequently, the wave packet on the excited state surface experiences several recurrences before being damped, and it samples information from a large region of the excited potential surface centered on the equilibrium geometry of the excited electronic state. This fact, together with the harmonicity of the corresponding excited state potential energy surfaces in that region, is most probably the reason the adiabatic method works well in the case of both electronic transitions of the bithiophene radical cation. On the other hand, the two experimental absorption bands have different appearances; the 425 nm band exhibits pronounced vibronic structure, while the 590 nm band is broad and unstructured. This difference manifests itself in the different values of the homogeneous line width used in the calculations for the two transitions. For the 590 nm band, a value of $\Gamma = 500$ cm^{-1} gave the best agreement between the calculated and observed absorption spectra, corresponding to an excited state lifetime of ~70 fs, whereas $\Gamma = 100$ cm^{-1} yielded the best results for the 425 nm band, indicating an excited state lifetime of ~330 fs. There is apparently a process that leads to the rapid depopulation of the 2^2A_u excited state. Internal conversion to an energetically close lying electronic state followed by vibrational relaxation is a likely explanation. According to our CASSCF calculations, at its optimized equilibrium geometry the 2^2A_u state has a negative Hessian eigenvalue, and at this geometry the energy separation between the 2^2A_u state and the lower lying 1^2A_u state is only 0.35 eV (~2850 cm^{-1}). Moreover, according to the state correlation diagram (Figure 5d), the two states exhibit an avoided crossing close to the s-trans structure.

In a preceding section, we have assigned the observed 590 and 425 nm absorption bands as the $1^2B_g \rightarrow 2^2A_u$ and $1^2B_g \rightarrow 3^2A_u$ transitions of the s-trans bithiophene radical cation, respectively, on the basis of the calculated oscillator strengths and transition energies. In the present section, we have demonstrated that the electronic absorption and resonance Raman spectra calculated on the basis of the vibrational parameters obtained for these states give good agreement with the experimental data. It is nevertheless also interesting to compare the observed Raman spectra with the calculated one, assuming the lowest ^2A_u state to be active in the resonance transition. The $1^2B_g \rightarrow 1^2A_u$ transition has a very low calculated oscillator strength, and it is predicted at 709 nm (1.75 eV). From the CASSCF calculated Hessians and gradients of this state, we can determine the vibrational parameters for both the adiabatic and the vertical approaches. In the absence of an experimental absorption band for this transition, we cannot obtain a fit of the transition energy and homogeneous damping factor. Thus, we are not able to perform a meaningful calculation of the Raman spectrum excited in resonance with this transition using the wave packet propagation method. Nevertheless, one can obtain a crude estimate of the resonance Raman intensities from the Savin formula. A resonance Raman spectrum calculated using the vertical Hessian approach and the Savin formula is shown in trace a of Figure 9, where it is compared to the experimental 550 nm (trace b) and 425 nm (trace c) excited spectra. It is seen that the calculated spectrum in trace a differs considerably from both experimental spectra, whereas the ones calculated by the same method for the $1^2B_g \rightarrow 2^2A_u$ and $1^2B_g \rightarrow 3^2A_u$ transitions, shown as traces b of Figures 7 and 8, respectively, showed reasonable agreement with experiment. This can be taken as further support of our assignment of the electronic absorption spectrum. We can also note here that the resonance Raman spectrum calculated using the adiabatic approach and the Savin formula (not shown here) is very much different form the vertical Hessian one in trace a of Figure 9, as could be expected on the basis of the different extrapolated and adiabatic geometries. Nonetheless, the adiabatic resonance Raman spectrum does not give better agreement with the experimental spectra than the vertical Hessian one.

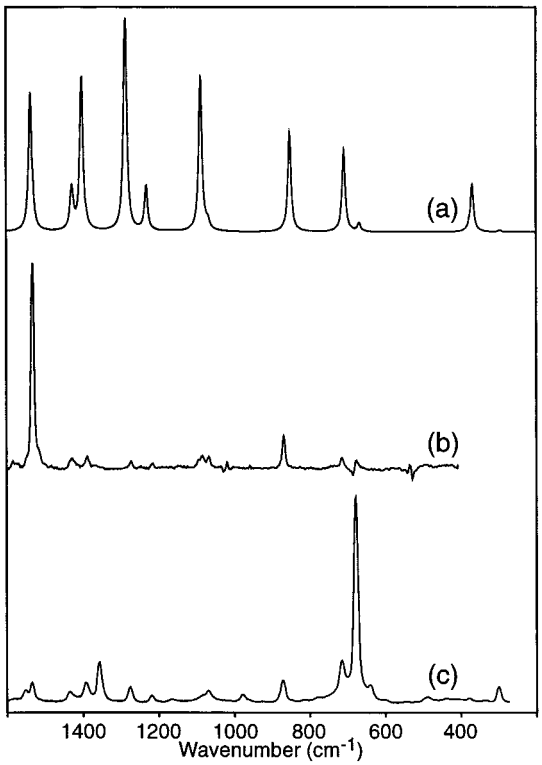

Figure 9. Experimental and simulated resonance Raman spectra of s-trans $2T^{+\cdot}$: (a) simulated spectrum for the $1^2B_g \rightarrow 1^2A_u$ transition using the vertical Hessian approach and the Savin formula; (b) experimental spectrum 550 nm excitation; (c) experimental spectrum 425 nm excitation.

Calculations on the s-cis Rotamer. In a previous section, we have assigned the observed electronic absorption and resonance Raman spectra to the s-trans rotamer of the bithiophene radical cation, with only one band in the 425 nm excited resonance Raman spectra attributed to the s-cis rotamer (ν_{13} at 640 cm^{-1}). In this section, we present the results of resonance Raman intensity calculations for the s-cis rotamer using the vertical Hessian method. Our linear response calculations have identified the $1^2A_2 \rightarrow 3^2B_1$ transitions of the s-cis rotamer (at 438 nm) as the one that might contribute to the 425 nm band in the absorption spectrum, and therefore the vibrational parameters for the intensity calculations have been obtained from CASSCF calculations on these states. We expect the absorption spectrum

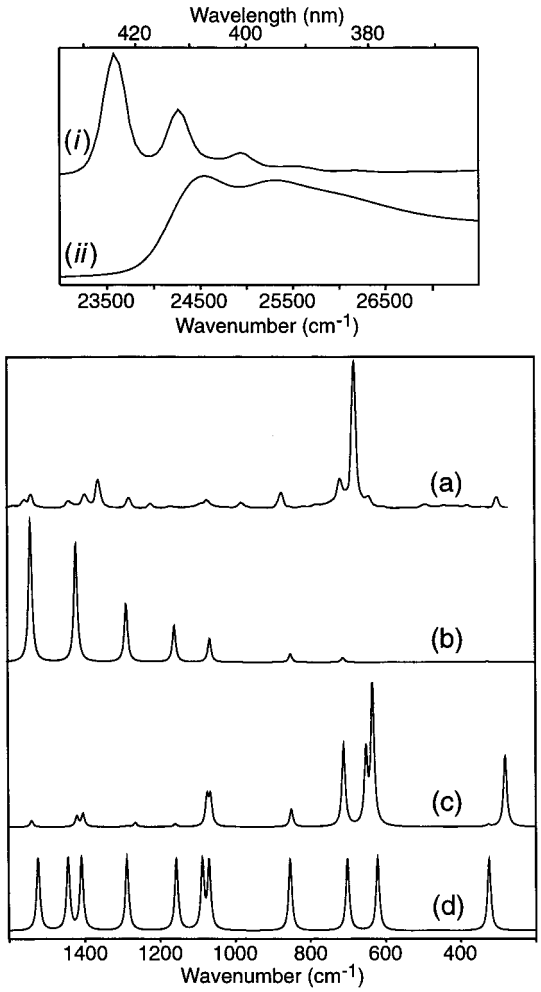

Figure 10. (upper window) Experimental and simulated electronic absorption spectra of s-cis $2T^{+\bullet}$ in the 23000−27500 cm^{-1} wavenumber range (435−364 nm): (i) experimental spectrum; (ii) calculated spectrum vertical Hessian approach (E_0 = 24028.5 cm^{-1}, Γ = 100 cm^{-1}). (lower window) Experimental and simulated 425 nm excited resonance Raman spectra of s-cis $2T^{+\bullet}$ in the 1600−200 cm^{-1} wavenumber range: (a) experimental spectrum; (b) calculated spectrum vertical Hessian approach using the Savin formula; (c) calculated spectrum vertical Hessian approach full time-domain calculation; (d) UB3-LYP calculated spectrum with uniform band intensities.

to derive primarily from the s-trans rotamer and to only contain a minor contribution from the s-cis rotamer; thus, we do not know the absorption spectrum of the pure s-cis rotamer. Therefore, we cannot obtain a fit of the transition energy and the homogeneous damping factor. It is, however, reasonable to assume that the difference between the CASSCF calculated and fitted transition energies is very similar for the two rotamers. Thus, from the CASSCF calculated vertical transition energies (27585.8 cm^{-1} for s-trans 27614.3 cm^{-1} s-cis) and the fitted E_0 of the s-trans rotamer (24000 cm^{-1} for the vertical Hessian calculations) we arrive at E_0 = 24028.5 cm^{-1} for the s-cis rotamer. Furthermore, we also assume that the homogeneous damping factor is the same for the 3^2B_1 state of the s-cis and the 3^2A_u state of the s-trans rotamer, and use the value of Γ = 100 cm^{-1} determined for the s-trans rotamer for our calculations on the s-cis rotamer.

The absorption spectrum calculated using these parameters (E_0 = 24028.5 cm^{-1}, Γ = 100 cm^{-1}) by the vertical Hessian method is shown in trace ii of the upper panel of Figure 10, where it is compared to the experimental spectrum (trace i). The lower panel of Figure 10 shows the calculated resonance Raman spectra for excitation at 425 nm. It is readily seen from Figure 10 that the both the absorption and the Raman spectra calculated for the s-cis rotamer are in much poorer agreement with the experimental ones than those calculated for the s-trans rotamer. It is also seen from the resonance Raman spectrum obtained by the full time domain calculation (trace c) that the strongest band is the one assigned to the ν_{13} fundamental (scaled CASSCF calculated wavenumber 631 cm^{-1}). A comparison of trace c of Figure 10 with trace c of Figure 8 shows that the other bands predicted to be fairly intense in the s-cis spectrum overlap with s-trans bands. For example, the calculations show it likely that the 300 cm^{-1} band assigned to ν_{14} (s-trans) has a contribution from the $2\times\nu_{15}$ (s-cis) mode, that the $2\times\nu_{14}$ (s-cis) band could be hidden in the shoulder of the intense ν_{13} (s-trans) band, and that the 488 cm^{-1} band, tentatively assigned to $2\times\nu_{42}$ (s-trans) , may also contain a contribution from the $\nu_{14} + \nu_{15}$ (s-cis) combination. The small band on the low-frequency side of the 872 cm^{-1} ν_{11} s-trans band could be assigned to the ν_{11} (s-cis) mode. However, these calculations are not sufficiently precise for such definite assignments of weak bands. We can nevertheless conclude that the calculated s-cis spectrum supports the assignment of the 640 cm^{-1} band to the ν_{13} (s-cis) mode. All other calculated bands of significant intensity can be hidden under s-trans bands or be small shoulder bands.

It is striking that the crude estimate based on the Savin formula (Figure 10, trace b) is completely wrong in this case. Comparing it with the full time domain calculations based on the vertical Hessian method (trace c), we see that here is *no* correlation between the calculated displacements and intensities in contrast to s-trans (Figure 8) which follows the more usual pattern. The Duschinsky rotation matrix is thus essential for a correct description of the resonance Raman spectrum of the s-cis rotamer. This illustrates that the simple and fast Savin formula must be used with caution, even for qualitative predictions. If the theoretical spectrum calculated using the Savin formula is in reasonable agreement with the experimental spectrum, it is a strong indication that the interpretation is correct, while negative predictions are much more dubious. From the Savin formula alone, one would have predicted that the 640 cm^{-1} band does definitely not derive from the s-cis rotamer!

Even though the 425 nm excited Raman spectrum is off-resonance for the s-cis rotamer, on the basis of the relative intensities of the 640 cm^{-1} (s-cis) and 678 cm^{-1} (s-trans) bands it appears that the concentration of the s-cis rotamer in the low-temperature samples is considerably lower than that of the s-trans rotamer. The s-cis rotamer thus only gives a minor contribution to the observed electronic absorption spectrum, which is therefore attributed to the s-trans rotamer. This conclusion is also supported by the calculations of the absorption spectra (cf. Figure 8, trace ii, and Figure 10, trace ii).

Implications for Polythiophene. As mentioned in the Introduction, our interest in the radical cation of bithiophene is in part due to its possible connection with the conductivity of polythiophene. Radical cations correspond to positive polarons, and it has recently been suggested[7] that polarons are the major charge carrying species existing in doped polythiophene. The electronic structures of polarons have mainly been discussed within the framework of a continuum electron−phonon coupled model.[3] According to this model, for a polaron two localized electronic levels appear within the gap, symmetrically around the gap center (see Figure 11). Thus, three intragap transitions are expected for a polaron, labeled p_1, p_2, and p_3 in Figure 10, and it has been predicted[27] that the oscillator strengths for the

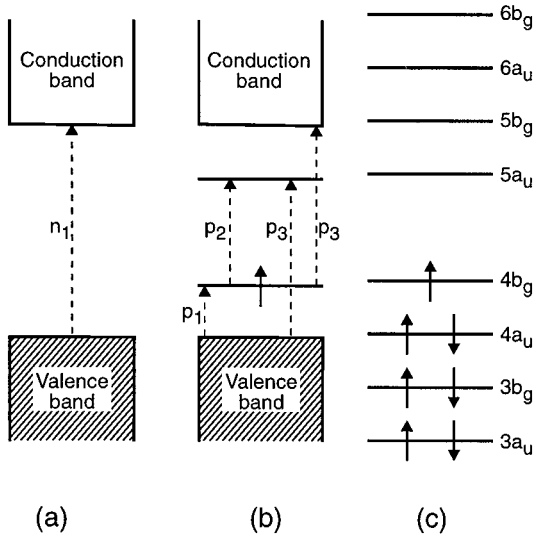

Figure 11. Schematic electronic level diagram for polythiophene in neutral (a) and positive polaron (b) state, together with the molecular orbital diagram of the bithiophene radical cation in the 1^2B_g ground state (c).

p_1 and p_2 transitions are much larger than for p_3. Our calculations for the bithiophene radical cation give a more complex picture. The CASSCF wave functions for the 2^2A_u and 3^2A_u states, which have been assigned as the excited states of the experimentally observed transitions, have major contributions from the $3a_u \rightarrow 4b_g$ and $4b_g \rightarrow 5a_u$ excitations, which can be related to the p_1 and p_2 transitions, respectively. However, both states have multiconfigurational character. Our calculations also predict the existence of a very low intensity transition to a lower lying electronic state, 1^2A_u, dominated by the $4a_u \rightarrow 4b_g$ excitation, which too can be related to the p_1 transition of a positive polaron. The existence of such a transition is not expected from the continuum electron−phonon coupled model. The p_3 transitions of the polaron correspond to excitations from the upper doubly occupied orbitals to the lowest unoccupied orbital (e.g., $3b_g \rightarrow 5a_u$) and from the highest, singly occupied orbital to other unoccupied orbitals (e.g., $4b_g \rightarrow 6a_u$). These excitations are expected to dominate high-lying excited states of the bithiophene radical cation, and such states have not been included in this study. The results of our work thus call for further theoretical studies into the electronic spectrum of longer thiophene oligomers in order to make a more clear connection with the electronic structure and optical absorptions of the polymer.

Summary and Conclusions

The bithiophene radical cation has been generated radiolytically in a low-temperature Freon glass, and its electronic absorption spectrum has been measured. The absorption spectrum exhibits a structured, intense band at 425 nm, and a broad unstructured band of lower intensity at 590 nm. Resonance Raman spectra have been measured using excitation within both absorption bands, at 425 nm and at 550 nm. Equilibrium geometries and vibrational frequencies of both rotamers, s-trans and s-cis, of the bithiophene radical cation have been obtained from density functional theory (UB-LYP and UB3-LYP/6-31G*) and ab initio (CASSCF/6-31G*) calculations. The calculated vibrational frequencies provide a good basis for the assignment of the Raman spectrum. We assign the resonance Raman spectrum to the more stable s-trans rotamer of the bithiophene radical cation, with only one band attributed to the s-cis rotamer. The concentration of the s-cis rotamer in the low temperature samples appears to be considerably lower than that of the s-trans rotamer. The s-cis rotamer also gives only a minor contribution to the observed electronic absorption spectrum. On the basis of transition energies and oscillator strengths from multiconfigurational linear response calculations, the two absorption bands at 590 and 425 nm have been unambiguously assigned to the $1^2B_g \rightarrow 2^2A_u$ and $1^2B_g \rightarrow 3^2A_u$ electronic transitions of the s-trans rotamer of the radical cation, respectively. Converged wave functions for the participating states have been obtained from CASSCF calculations, and geometry optimizations at this level of theory have been carried out as well. From the CASSCF calculated gradients and Hessian matrices vibrational parameters (normal coordinates, vibrational frequencies, dimensionless displacements, and the Duschinsky rotation matrix) are obtained for subsequent calculations of the optical absorption spectra and resonance Raman intensities by means of wave packet propagation techniques. Two different approaches, denoted as adiabatic and vertical, have been employed for the determination of the vibrational parameters. The Savin formula has also been used to estimate resonance Raman intensities. According to our results, the absorption and resonance Raman spectra calculated for the two electronic transitions of the s-trans rotamer using both the adiabatic and the vertical approaches give satisfactory agreement with the experimentally observed spectra. This implies that the potential energy surfaces of the 2^2A_u and 3^2A_u states do not deviate substantially from harmonicity in the region between the geometry of the 1^2B_g ground state and their respective equilibrium geometries. The Savin formula, as it is expected, performs fairly well for of the unstructured 590 nm absorption band and more poorly the in the case structured 425 nm band of the s-trans rotamer, while quite unexpectedly it gives completely wrong results for the s-cis rotamer.

References and Notes

(1) Skotheim, T. J., Ed. *Handbook of Conducting Polymers*; Marcel Dekker: New York, 1986; Vols. 1 and 2.

(2) (a) Berggren, M.; Inganäs, O.; Gustafsson, G.; Rasmusson, J.; Andersson, M. R.; Hjertberg, T.; Wennerström, O. *Nature* **1994**, *372*, 444. (b) Granström, M.; Berggren, M.; Inganäs, O. *Science* **1995**, *267*, 1479.

(3) Heeger, A. J.; Livelson, S.; Schrieffer, J. R.; Su, W.-P. *Rev. Mod. Phys.* **1988**, *60*, 781.

(4) Evans, C. H.; Scaiano, J. C. *J. Am. Chem. Soc.* **1990**, *112*, 2694.

(5) Wintgens, V.; Valat, P.; Garnier, F. *J. Phys. Chem.* **1994**, *98*, 228.

(6) Lanzani, G.; Rossi, L.; Piaggi, A.; Pal, A. J.; Taliani, C. *Chem. Phys. Lett.* **1994**, *226*, 547.

(7) Yokonuma, N.; Furukawa, Y.; Tasumi, M.; Kuroda, M.; Nakayama, J. *Chem. Phys. Lett.* **1996**, *255*, 431.

(8) Yu, Y.; Gunic, E.; Zinger, B.; Miller, L. L. J. *Am. Chem. Soc.* **1996**, *118*, 1013.

(9) (a) Ehrendorfer, C.; Karpfen, A. *J. Phys. Chem.* **1995**, *99*, 5341. (b) Tol, A. J. W. *Chem. Phys.* **1996**, *208*, 73. (c) Aleman, C.; Julià, L. *J. Phys. Chem.* **1996**, *100*, 14661.

(10) (a) Hill, M. G.; Mann, K. R.; Miller, L. L.; Penneau, J.-F. *J. Am. Chem. Soc.* **1992**, *114*, 2728. (b) Hill, M.G.; Penneau, J.-F.; Mann, K. R.; Miller, L. L. *Chem. Mater.* **1992**, *4*, 1106.

(11) Grage, M. M.-L.; Keszthelyi, T.; Offersgaard, J. F.; Wilbrandt, R. *Chem. Phys. Lett.* **1997**, *282*, 171.

(12) Frisch, M. J.; Trucks, G. W.; Schlegel, H. B.; Gill, P. M. W.; Johnson, B. G.; Robb, M. A.; Cheeseman, J. R.; Keith, T.; Petersson, G. A.; Montgomery, J. A.; Raghavachari, K.; Al-Laham, M. A.; Zakrzewski, V. G.; Ortiz, J. V.; Foresman, J. B.; Cioslowski, J.; Stefanov, B. B.; Nanayakkara, A.; Challacombe, M.; Peng, C. Y.; Ayala, P. Y.; Chen, W.; Wong, M. W.; Andres, J. L.; Replogle, E. S.; Gomperts, R.; Martin, R. L.; Fox, D. J.; Binkley, J. S.; Defrees, D. J.; Baker, J.; Stewart, J. P.; Head-Gordon, M.; Gonzalez, C.; Pople, J. A. *Gaussian 94*, revision B.1; Gaussian, Inc.: Pittsburgh, PA, 1995.

(13) (a) Jensen, H. J. Aa.; Jørgensen, P.; Ågren, H.; Olsen, J. *J. Chem. Phys.* **1988**, *88*, 3834. (b) Jensen, H. J. Aa.; Jørgensen, P.; Ågren, H.; Olsen, J. *J. Chem. Phys.* **1988**, *89*, 5354.

(14) Helgaker, T.; Jensen, H. J. Aa.; Jørgensen, P.; Olsen, J.; Ruud, K.; Ågren, H.; Andersen, T.; Bak, K. L.; Bakken, V.; Christiansen, O.; Dahle,

P.; Dalskov, E. K.; Enevoldsen, T.; Fernandez, B.; Heiberg, H.; Hettema, H.; Jonsson, D.; Kirpekar, S.; Kobayashi, R.; Koch, H.; Mikkelsen, K. V.; Norman, P.; Packer, M. J.; Saue, T.; Taylor, P. R.; Vahtras, O. *Dalton*, release 1.0; 1997 (an electronic structure program).

(15) Samdal, S.; Samuelsen, E. J.; Volden, H. V. *Synth. Met.* **1993**, *59*, 259.

(16) Ortí, E.; Viruela, P. M.; Sánchez-Marín, J.; Tomás, F. *J. Phys. Chem.* **1995**, *99*, 4955.

(17) Viruela, P. M.; Viruela, R.; Ortí, E.; Brédas, J.-L. *J. Am. Chem. Soc.* **1997**, *119*, 1360.

(18) Chadwick, J. E.; Kohler, B. E. *J. Phys. Chem.* **1994**, *98*, 3631.

(19) Keszthelyi, T.; Wilbrandt, R.; Bally, T. *J. Mol. Struct.* **1997**, *410*−*411*, 339 and references therein.

(20) Bally, T.; Nitsche, S.; Roth, K.; Haselbach, E. *J. Phys. Chem.* **1985**, *89*, 2528.

(21) Jørgensen, P.; Jensen, H. J. Aa.; Olsen, J. *J. Chem. Phys.* **1988**, *89*, 3654.

(22) (a) Brouwer, A. M.; Svendsen, C.; Mortensen, O. S.; Wilbrandt, R. *J. Raman. Spectrosc.* **1998**, *29*, 439. (b) Brouwer, A. M.; Zwier, J. M.; Svendsen, C.; Mortensen, O. S.; Langkilde, F. W.; Wilbrandt, R. *J. Am. Chem. Soc.* **1998**, *120*, 3748.

(23) (a) Lee, S. Y.; Heller, E. J. *J. Chem. Phys.* **1979**, *71*, 4777. (b) Heller, E. J.; Sundberg, R. L.; Tannor, D. *J. Phys. Chem.* **1982**, *86*, 1822. (c) Tannor, D. J.; Heller, E. J. *J. Chem. Phys.* **1982**, *77*, 202. (d) Heller, E. J. *J. Chem. Phys.* **1978**, *68*, 3891. (e) Heller, E. J. *Acc. Chem. Res.* **1981**, *14*, 368.

(24) Svendsen, C.; Mortensen, O. S.; Henriksen, N. E. *Chem. Phys. Lett.* **1996**, *260*, 627.

(25) Warshel, A.; Karplus, M. *Chem. Phys. Lett.* **1972**, *17*, 7.

(26) (a) Myers, A. B. *Chem. Rev.* **1996**, *96*, 911. (b) Lee, S. Y.; Lee, S. C. *J. Phys. Chem.* **1992**, *96*, 5734. (c) Wootton, J. L.; Zink, J. I. *J. Am. Chem. Soc.* **1997**, *119*, 1895.

(27) Fesser, K.; Biskop, A. R.; Campbell, D. K. *Phys. Rev.* **1983**, *B27*, 4804.